PB84-184753

Development of the Mesopuff II Dispersion Model

Environmental Research and Technology, Inc.
Concord, MA

Prepared for

Environmental Sciences Research Lab.
Research Triangle Park, NC

Apr 84

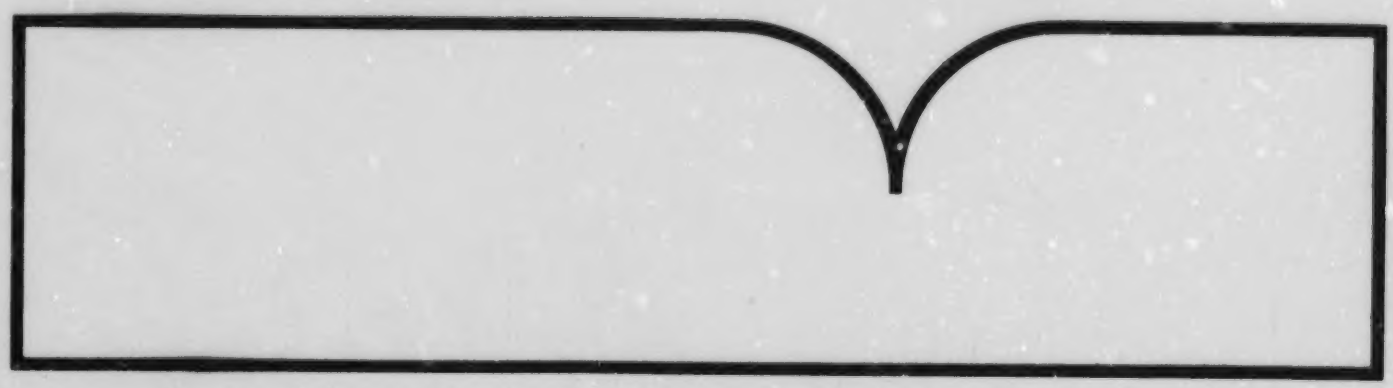

U.S. Department of Commerce
National Technical Information Service
NTIS

PB84-184753

EPA-600/3-84-057
April 1984

DEVELOPMENT OF THE MESOPUFF II DISPERSION MODEL

by

Joseph S. Scire
Frederick W. Lurmann
Arthur Bass
Steven R. Hanna
Environmental Research & Technology, Inc.
Concord, Massachusetts 01742

Contract No. 68-02-3733

Project Officer

James M. Godowitch
Meteorology and Assessment Division
Environmental Sciences Research Laboratory
Research Triangle Park, NC 27711

ENVIRONMENTAL SCIENCES RESEARCH LABORATORY
OFFICE OF RESEARCH AND DEVELOPMENT
U.S. ENVIRONMENTAL PROTECTION AGENCY
RESEARCH TRIANGLE PARK, NC 27711

REPRODUCED BY
NATIONAL TECHNI
INFORMATION SER
U.S. DEPARTMENT OF COMMERC
SPRINGFIELD, VA. 22161
REPRODUCED
NATIC
INFOR
U.S. D
SPR

TECHNICAL REPORT DATA *(Please read Instructions on the reverse before completing)*		
1. REPORT NO. EPA-600/3-84-057	2.	3. RECIPIENT'S ACCESSION NO. PB84 183753
4. TITLE AND SUBTITLE DEVELOPMENT OF THE MESOPUFF II DISPERSION MODEL		5. REPORT DATE April 1984
		6. PERFORMING ORGANIZATION CODE
7. AUTHOR(S) J. S. Scire, F. W. Lurmann, A. Bass, S. R. Hanna		8. PERFORMING ORGANIZATION REPORT NO.
9. PERFORMING ORGANIZATION NAME AND ADDRESS Environmental Research & Technology, Inc. 696 Virginia Road Concord, Massachusetts 01742		10. PROGRAM ELEMENT NO. CDTA1D/02-1607 (FY-84)
		11. CONTRACT/GRANT NO. 68-02-3733
12. SPONSORING AGENCY NAME AND ADDRESS Environmental Sciences Research Laboratory--RTP, NC Office of Research and Development U.S. Environmental Protection Agency Research Triangle Park, NC 27711		13. TYPE OF REPORT AND PERIOD COVERED Final
		14. SPONSORING AGENCY CODE EPA/600/09
15. SUPPLEMENTARY NOTES		

16. ABSTRACT

The development of the MESOPUFF II regional-scale air quality model is described. MESOPUFF II is a Lagrangian variable-trajectory puff superposition model suitable for modeling the transport, diffusion and removal of air pollutants from multiple point and area sources at transport distances beyond the range of conventional straight-line Gaussian plume models (i.e., beyond ~ 10-50 km). It is an extensively modified version of the MESOscale PUFF (MESOPUFF) model. Major additions and enhancements include: use of hourly surface meteorological data and twice-daily rawinsonde data; separate wind fields to represent flow within and above the boundary layer; parameterization of vertical dispersion in terms of micrometeorological turbulence variables; parameterization of SO_2 to $SO_4^=$ and NO_x to NO_3^- conversion, including the chemical equilibrium of the $HNO_3/NH_3/NH_4NO_3$ system; resistance modeling of dry deposition, including options for source or surface depletion; time- and space-varying wet removal; and a computationally efficient puff sampling function. The scientific and operational bases for these developments are described. The results of a preliminary evaluation of several model algorithms during a two-day period of the Tennessee Plume Study are also presented.

17. KEY WORDS AND DOCUMENT ANALYSIS		
a. DESCRIPTORS	b. IDENTIFIERS/OPEN ENDED TERMS	c. COSATI Field/Group
18. DISTRIBUTION STATEMENT RELEASE TO PUBLIC	19. SECURITY CLASS *(This Report)* UNCLASSIFIED	21. NO. OF PAGES 91
	20. SECURITY CLASS *(This page)* UNCLASSIFIED	22. PRICE

EPA Form 2220-1 (9-73)

NOTICE

This document has been reviewed in accordance with U.S. Environmental Protection Agency policy and approved for publication. Mention of trade names or commercial products does not constitute endorsement or recommendation for use.

PREFACE

This publication contains a technical description of the MESOPUFF II model and its processor programs. The preprocessor programs require hourly meteorological surface, twice-daily upper air, and hourly precipitation (optional) data in the formats archived by the National Climatic Center in Asheville, North Carolina. The model utilizes the Gaussian puff superposition approach to simulate a continuous pollutant plume. The model is capable of multi-day simulations and has algorithms for plume rise, transport, chemical transformations, dry deposition, and wet removal. Terrain variations are not accounted for in the model.

The puff superposition approach has not been used extensively in air quality models for the prediction of pollutant concentrations. MESOPUFF II is being made available to promote testing and evaluation of the methods and optional features in the model. MESOPUFF II has no regulatory standing and its application for regulatory purposes should be considered in light of EPA's Guideline on Air Quality Models.

The model version (1.0) documented in this publication represents an attempt to utilize recent scientific information to realistically account for the relevant physical processes active on the regional to long-range scales. Modifications may be made in the future based on results by users and findings from ongoing research programs.

Although attempts have been made to check the computer program code, errors may be found occasionally. Adjustments to the code to suit different computer systems may be required. If there is a need to correct, revise, or update this model, changes may be obtained as they are issued by completing and sending the form on the last page of the user guide.

It is anticipated that MESOPUFF II will be made available in the future on the User's Network for Applied Modeling of Air Pollution (UNAMAP) system. A tape of this model or the UNAMAP system may be purchased from NTIS for use on the user's computer system. For information on UNAMAP contact: Chief, Environmental Operations Branch, MD-80, U.S. Environmental Protection Agency, Research Triangle Park, NC 27711.

ABSTRACT

The development of the MESOPUFF II regional-scale air quality model is described. MESOPUFF II is a Lagrangian variable-trajectory puff superposition model suitable for modeling the transport, diffusion and removal of air pollutants from multiple point and area sources at transport distances beyond the range of conventional straight-line Gaussian plume models (i.e., beyond ∿ 10-50 km). It is an extensively modified version of the MESOscale PUFF (MESOPUFF) model (Benkley and Bass 1979). Major additions and enhancements include: use of hourly surface meteorological data and twice-daily rawinsonde data; separate wind fields to represent flow within and above the boundary layer; parameterization of vertical dispersion in terms of micrometeorological turbulence variables; parameterization of SO_2 to $SO_4^=$ and NO_x to NO_3^- conversion, including the chemical equilibrium of the $HNO_3/NH_3/NH_4NO_3$ system; resistance modeling of dry deposition, including options for source or surface depletion; time- and space-varying wet removal; and a computationally efficient puff sampling function. The scientific and operational bases for these developments are described. The results of a preliminary evaluation of several model algorithms during a two-day period of the Tennessee Plume Study are also presented.

This report was submitted in fulfillment of Contract No. 68-02-3733 by Environmental Research & Technology, Inc. under sponsorship of the U.S. Environmental Protection Agency. This report covers the period from February 11, 1982 to March 15, 1983, and work was completed as of September, 1983.

CONTENTS

Preface iii
Abstract iv
Figures vi
Tables vii
Acknowledgements viii

1. Introduction 1
   1.1 Background 1
   1.2 MESOPUFF II Modeling Package 2
   1.3 Major Features of MESOPUFF II 4
   1.4 Tennessee Plume Study 8
2. Technical Developments 10
   2.1 Wind Field 10
   2.2 Micrometeorological Parameters 14
   2.3 Dry Deposition - Three Layer Model 21
   2.4 Chemical Transformations 33
   2.5 Wet Removal 50
   2.6 Puff Sampling Function 55
3. Demonstration Model Run 62
References 72
Appendices

   A. Reactions and rate constants of the Atkinson et al. (1982) chemical mechanism 77

FIGURES

Number		Page
1	MESOPUFF II Modeling Package	3
2	Schematic Representation of Puff Superposition Approach	5
3	Particle Deposition to Water Surfaces	24
4	SO_2 Deposition Velocities	25
5	Comparison of Source Depletion and Surface Depletion Models	31
6	Optional Three Layer System Used in MESOPUFF II.	32
7	SO_2 Oxidation Pathways	35
8	NO_x Oxidation Pathways	36
9	NH_4NO_3 Dissociation Constant Temperature and Relative Humidity Dependence	39
10	Comparison of SO_2 Oxidation Rates Predicted by the ERT and Gillani et al. Equations	47
11	Average Plume Sulfur Conversion Rate as a Function of Mean Time of Day of Plume Transport	48
12	Washout Ratio as a Function of Precipitation Rate for Different Storm Types	51
13	SO_2 Washout Ratio as a Function of pH and Temperature for Equilibrium Scavenging Conditions	53
14	Location of Cumberland Steam Plant, Surface Meteorological Stations and Upper Air Rawinsonde Stations on Meteorological Grid.	64
15	Boundary Layer Growth and Plume Fumigation	67
16	Observed and Predicted Mixing Heights in the Vicinity of the Cumberland Steam Plant	68

TABLES

Number		Page
1	Major Features of MESOPUFF II	7
2	Options for Lower and Upper Wind Fields	12
3	Solar Radiation Reduction Factor B	17
4	Factors Influencing Dry Deposition Removal Rates. .	22
5	Summertime SO_2 Canopy Resistances as a Function of Land Use Type and Stability Class . .	28
6	Parameter Variations in the Photochemical Modeling Simulations	43
7	Default Values of the Scavenging Coefficient, λ (s^{-1})	54
8	Conversion of Reported Precipitation Type/ Intensity to Precipitation Codes	56
9	Effect of Sampling Rate, N, on Predicted Near-Field Concentrations for Two Sampling Algorithms.	60
10	Model Run Parameters Used in Demonstration Run. . .	65
11	History of Puff Released 8/23/78 Hour 1	66
12	Observed and Predicted SO_2 Conversion Rates	70

ACKNOWLEDGEMENTS

The authors wish to acknowledge the contributions made by Drs. A. Venkatram and R. Yamartino to the development of MESOPUFF II. The assistance and advice of the EPA project officer, James Godowitch, is appreciated.

SECTION 1
INTRODUCTION

1.1 Background

The regional and long-range transport and transformation of sulfur oxides and nitrogen oxides emitted from major point sources are of increasing concern. Motivated by the need for easily-used, cost-efficient mesoscale air quality models suitable for regulatory applications, the National Oceanic and Atmospheric Administration (NOAA) sponsored a study by Environmental Research & Technology, Inc. (ERT) to develop, compare, and evaluate a set of mesoscale models and related processor programs known as the MESO-models (Benkley and Bass 1979a, b, c; Morris et al. 1979; Scire et al. 1979). One of these models, the MESOscale PUFF (MESOPUFF) model appears to be well suited for regulatory use. For this reason, the Environmental Protection Agency (EPA) has sponsored a second study by ERT to enhance the capabilities and flexibility of the MESOPUFF model to meet the current and future needs of EPA in predicting mesoscale transport of pollutants, especially secondary aerosols.

This report is the first volume of a two-volume set describing the results of this effort to extent MESOPUFF's capabilities. Extensive modifications have been made to MESOPUFF in order to refine and enhance its treatment of advection, vertical dispersion, removal and transformation processes. The new model has been designated MESOPUFF II. The objective of this document is to describe the scientific and operational bases for the most significant modifications made to MESOPUFF. In addition, this document provides the results of a demonstration run of the model for a two-day period during the Tennessee Plume Study (TPS). The companion report, entitled "User's Guide to the MESOPUFF II Model and Related Processor Programs" provides a summary of the basic model equations and includes a

complete set of user instructions for the MESOPUFF II model and its processor programs (READ56, MESOPAC II, MESOFILE II). The User's Guide also contains a description of several model algorithms not presented in this document that were unchanged or only slightly modified (e.g., the puff trajectory function, dispersion coefficient calculations and the plume rise algorithm).

In the next section, the MESOPUFF II modeling package is outlined and the functions of each program are discussed. Section 1.3 contains a summary of the major modifications made in MESOPUFF II. The TPS is briefly described in Section 1.4. The second chapter contains a technical description of model algorithms. A description of a demonstration run of the model for two days during the TPS and the results are contained in the third chapter.

1.2 MESOPUFF II Modeling Package

The MESOPUFF II model is one element of an integrated modeling package. This modeling package (Figure 1) also contains components for preprocessing of meteorological data (READ56, MESOPAC II) and postprocessing of predicted concentration results (MESOFILE II). Each component of the MESOPUFF II modeling package is briefly described below.

READ56 is a preprocessor program that reads and processes the twice-daily upper air wind and temperature sounding data available from the National Climatic Center (NCC) for selected stations. READ56 extracts the data required by the MESOPAC II program from a standard-formatted NCC tape (TDF5600). READ56 scans the upper air data for completeness; warning messages are printed to flag missing or incomplete soundings. A file of processed sounding data is created in a format convenient for possible editing by the user and it is subsequently input into the MESOPAC II program.

MESOPAC II is the meteorological processor program that computes the time and space interpolated fields of meteorological variables (e.g., transport winds, mixing height) required by MESOPUFF II to describe

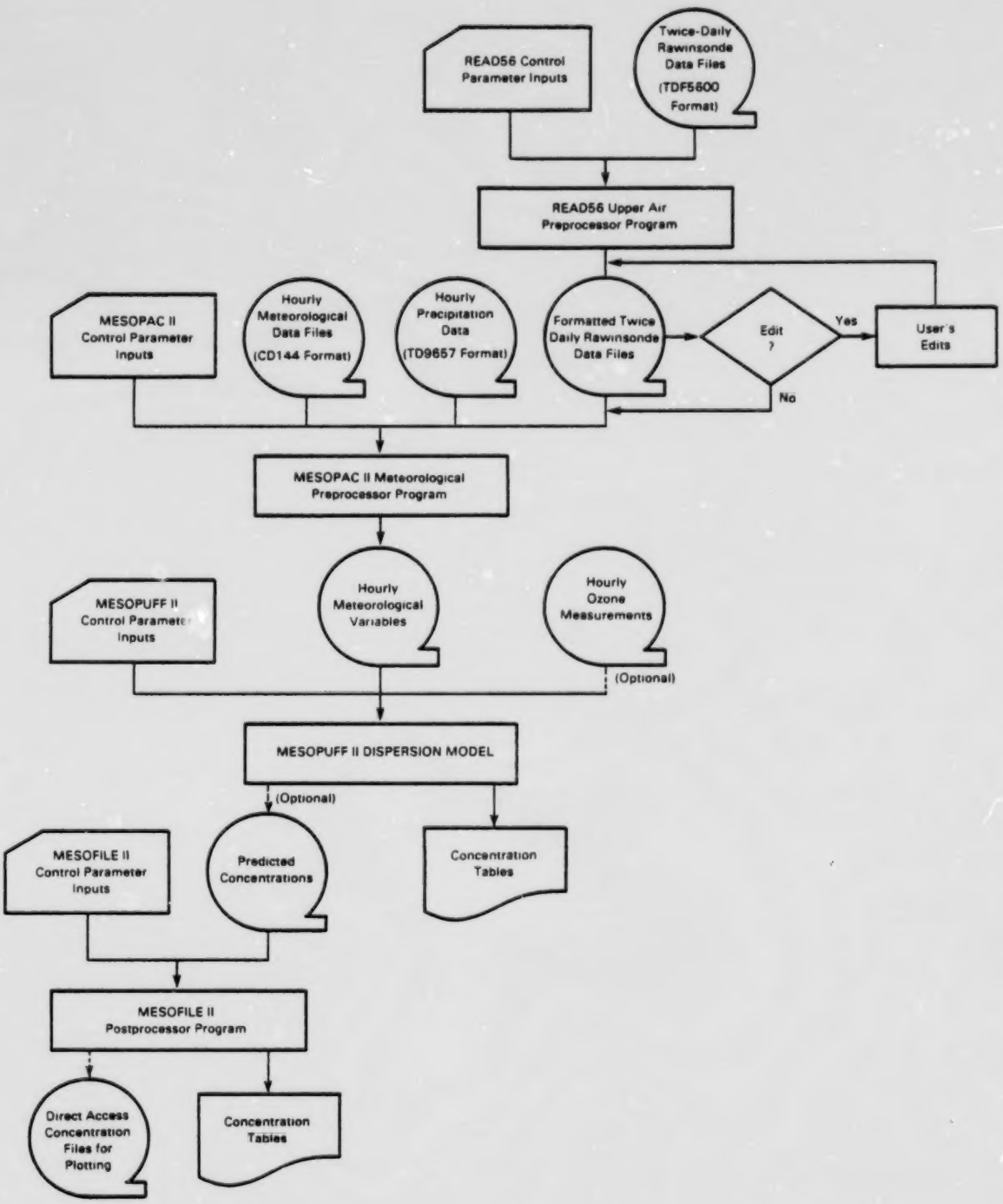

Figure 1 MESOPUFF II Modeling Package

mesoscale transport and dispersion processes. MESOPAC II reads the upper air data files created by READ56 and files of standard-formatted NCC hourly surface meteorological data (CD144) and hourly precipitation data (TD9657). A single output file containing observed and derived meteorological fields is produced which serves as an input file to MESOPUFF II.

MESOPUFF II is a Gaussian, variable-trajectory, puff superposition model designed to account for the spatial and temporal variations in transport, diffusion, chemical transformation and removal mechanisms encountered on regional scales. With the puff superposition approach, a continuous plume is modeled as a series of discrete puffs (Figure 2). Each puff is transported independently of other puffs. A puff is subject to growth by diffusion, chemical transformations, wet removal by precipitation, and dry deposition at the surface. Up to five pollutants may be modeled simultaneously.

MESOFILE II is a postprocessing program that operates on the concentration file produced by MESOPUFF II. The postprocessing functions available with MESOFILE II include flexible time averaging of gridded or non-gridded (discrete) receptor concentrations, line printer contour plots of concentration fields, statistical analysis of point-by-point or bulk differences between concentration fields, and summing and scaling capabilities.

1.3 Major Features of MESOPUFF II

The original MESOPUFF model is a single-layer, two species puff superposition model. Its meteorological preprocessor (MESOPAC) creates gridded fields of wind components, mixing height, and stability class from twice-daily rawinsonde (upper air) data. Chemical transformation of sulfur dioxide to sulfate is modeled with a spatially and temporally constant transformation rate. Dry deposition is modeled with a constant deposition velocity for each pollutant by the source depletion technique.

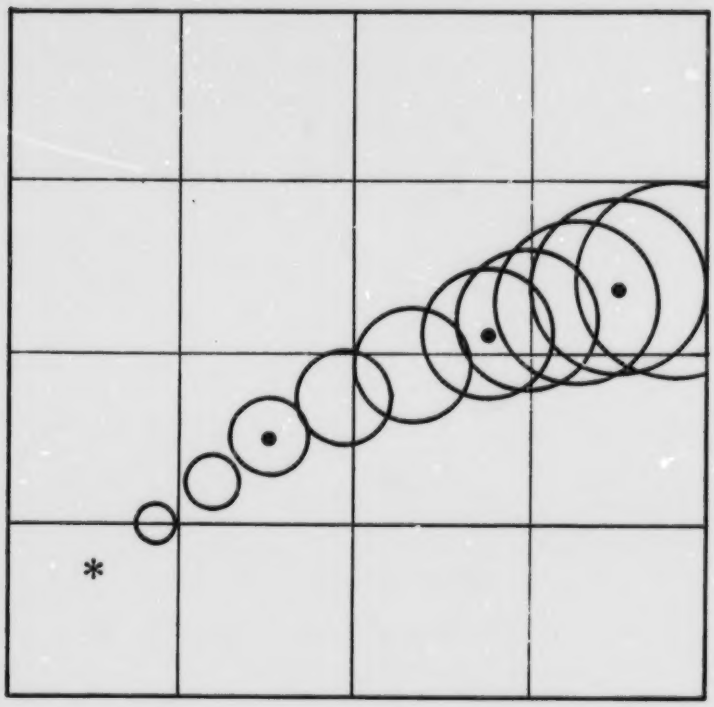

Figure 2 Schematic Representation of Puff Superposition Approach

807090

Table 1 outlines the most important modifications made in MESOPUFF II and its processor programs. Each of these changes is discussed in detail in Chapter 2. MESOPAC II supplements twice-daily rawinsonde data with hourly surface data to construct wind fields at two levels. The greater temporal and spatial resolution of the surface data allows improved treatment of plume transport. Wind fields are determined at two user-selected levels; a lower level to represent boundary layer flow and an upper level to represent flow above the boundary layer.

The additional information contained in the surface meteorological observations allows calculation of important micrometeorological variables that determine the structure of the boundary layer (i.e., surface friction velocity, u_*, convective velocity scale, w_*, Monin-Obukhov length, L, and boundary layer height, z_i). These variables are computed by MESOPAC II from surface meteorological data and surface characteristics (i.e., land use, roughness length) provided by the user for each grid point.

MESOPUFF II has been expanded to accommodate up to five pollutants: sulfur dioxide (SO_2), sulfate ($SO_4^=$), nitrogen oxides (NO_x = NO + NO_2), nitric acid (HNO_3), and nitrate (NO_3^-). Chemical transformation rate expressions have been developed from the results of photochemical model simulations over a wide range of environmental conditions. The rate expressions include gas phase NO_x oxidation, and gas/aqueous phase SO_2 oxidation. The $HNO_3/NH_3/NH_4NO_3$ chemical equilibrium relationship has also been incorporated into the model.

The dry deposition of pollutants is treated in MESOPUFF II with a resistance model. The pollutant flux is proportional to the inverse of a sum of resistances of pollutant transfer through the atmosphere to the surface. The resistances depend on the characteristics of the pollutant, the underlying surface, and atmospheric conditions. MESOPUFF II contains options for the commonly used source depletion method of pollutant removal by dry deposition (i.e., pollutant is removed from the entire depth of the puff) or the more realistic surface depletion treatment (i.e., material is removed only from the surface layer) with a 3-layer submodule.

TABLE 1. MAJOR FEATURES OF MESOPUFF II

- Uses hourly surface meteorological data and upper air rawinsonde data
- Wind fields constructed for two layers (within boundary layer, above boundary layer)
- Boundary layer structure parameterized in terms of micrometeorological variables u_*, w_*, z_i, L
- Up to five species (e.g., SO_2, $SO_4^=$, NO_x, HNO_3, NO_3^-)
- Space- and time-varying chemical transformations
- Space- and time-varying dry deposition; resistance model; source or surface depletion
- Space and time-varying wet removal
- Efficient puff sampling function.

Precipitation scavenging is frequently the dominant pollutant removal mechanism during precipitation periods. MESOPUFF II contains a scavenging ratio formulation for wet removal. The scavenging ratio depends on both the type and rate of precipitation, and the characteristics of the pollutant.

Improvements in MESOPUFF II have been made in the method which evaluates and sums the contributions of individual puffs to the total concentration. The model uses an integrated form of the puff sampling function that eliminates the problem of insufficient puff overlap commonly encountered with puff superposition models. This development allows continuous plumes to be accurately simulated with fewer puffs, thereby saving computational time and reducing computer storage requirements.

1.4 Tennessee Plume Study

The TPS was conducted in August 1978 as part of EPA's Sulfur Transport and Transformation in the Environment (STATE) program. The experimental study was conducted in the vicinity of the TVA Cumberland Steam Plant. The Cumberland Plant is a base load 2600 MW plant which is located in northwestern Tennessee. Although sampling the Cumberland plume was the main objective of the experiment, plume measurements from other TVA plants (e.g., Johnsonville, Paradise and Gallatin) were made when they were transported near the Cumberland plume. The trajectory of the Cumberland plume was determined by tracking tetroons, a manned LAMP balloon, and ground and airborne sampling of a tracer gas (SF_6). Dispersion and chemical measurements were obtained by aircraft and ground-based mobile vans. Four specific scenarios were studied:

- Vertical mixing during highly convective conditions to downwind distances of 50 km.
- Horizontal plume spread during stable conditions with significant wind shear to downwind distances of 300-500 km. The initial plume is emitted into the mixed layer.
- Dispersion during stable conditions to distances of 400 km. The initial plume is emitted into a stable layer.

- Dispersion and chemical changes over a diurnal cycle, with fumigation in the morning and layering in the evening.

Although a detailed evaluation of MESOPUFF II with the TPS data base is beyond the scope of the current study, a demonstration run for a two-day period during the TPS has been made. The purposes of the demonstration run were to allow a preliminary assessment of the SO_2 to $SO_4^=$ chemical transformation formulation for one of the scenarios (Scenario 4) and to qualitatively demonstrate the behavior of several other model algorithms.

SECTION 2
TECHNICAL DEVELOPMENTS

2.1 Wind Fields

A principal concern in long range transport modeling is the spatial and temporal resolution of the data used to construct the wind field for plume advection. The spatial resolution of routinely available NWS rawinsonde data is only marginally adequate for long range transport modeling. The typical distance between rawinsonde stations is 300-500 kilometers. Another limitation is the poor temporal resolution of the routinely available twice-daily sounding data. Important variations in the wind field, mixing height, and atmospheric stability occur on much smaller space- and time-scales than those resolvable by the NWS upper-air sounding network.

To increase the spatial and temporal resolution of the meteorological data used in MESOPUFF II and to obtain a better representation of the boundary layer flow, the meteorological preprocessor program has been modified to allow the twice-daily upper air data to be supplemented with hourly surface data from the much denser network of NWS surface stations. In addition, wind fields are constructed at two levels: a lower level field representing boundary layer flow, and an upper level wind field representing flow above the boundary layer. The lower level winds are used to advect puffs within the mixed layer and to determine the plume rise of newly released puffs. The upper level winds are used to advect puffs which are above the boundary layer. At each time step, the appropriate wind field for advection of a puff is determined by comparison of the height of the puff center with the spatially and temporally varying mixing height. If the puff center is above (below) the mixing height at the closest grid point, the entire puff is advected with the upper (lower) level wind.

Considerable flexibility is allowed in choosing the most appropriate level or vertically-averaged layer for each wind field. Table 2 contains the available options. The default instructions are to use the winds averaged through the mixed layer for the lower level wind field, and the wind averaged from the top of the mixed layer through the 700 mb level (~ 3000 m) for the upper level wind field. However, if desired, the user may select other levels to determine the wind fields (e.g., surface and 850 mb levels). The model may be made a single wind field model by specifying the lower and upper wind fields to be the same.

The mixed layer averaged winds are calculated from twice-daily rawinsonde data from upper air stations and hourly surface data from the typically much denser network of surface stations. Layer-averaged wind speed and wind direction computed from the rawinsonde data are used to adjust the hourly surface winds. The following five step procedure, adapted from Draxler (1979), is used to determine the mixed layer wind at each point:

(1) A representative rawinsonde sounding (00 or 12 GMT) is selected based upon the stability class at the nearest surface station to the grid point and the time of day. Neutral/unstable and stable conditions are assumed to be represented by the 00 GMT and 12 GMT sounding, respectively.

(2) Using the sounding selected in Step (1), vertically averaged u (easterly) and v (northerly) wind components are computed through the layer from the surface to the grid point mixing height.

(3) The ratio, R, of the layer-averaged wind speed to the surface wind speed at the rawinsonde station, and the angular difference in wind direction, $\Delta\theta$, between the layer averaged and surface winds are calculated.

(4) The hourly surface wind data are used to calculate spatially interpolated surface wind components (u_s, v_s) at each grid point. Data from all surface stations within a user-specified

TABLE 2. OPTIONS FOR LOWER AND UPPER WIND FIELDS

Option	Meteorological Data
Vertically Averaged Winds	
Surface to mixing ht [1]	Surface, Rawinsonde
Mixing ht to 850 mb	Rawinsonde
Mixing ht to 700 mb [2]	Rawinsonde
Mixing ht to 500 mb	Rawinsonde
Single Level Winds	
Surface	Surface
850 mb	Rawinsonde
700 mb	Rawinsonde
500 mb	Rawinsonde

[1] Default lower level wind field
[2] Default upper level wind field

'scan-radius' of a grid point are used to compute (u_s, v_s) according to

$$(u_s, v_s)_{ij} = \frac{\sum_k \frac{\alpha_s}{r_s^2} \cdot (u_k, v_k)}{\sum_k \frac{\alpha_s}{r_s^2}} \qquad (2\text{-}1)$$

where u_s, v_s are the easterly and northerly components of the surface wind at grid point (i, j),

u_k, v_k are the easterly and northerly components of the surface wind at surface station k,

r_s is the distance from the surface station to grid point (i, j), and

α_s is an alignment weighting factor ($\alpha_s = 1\text{-}0.5\,|\sin \phi_s|$, where ϕ_s is the angle between the observed wind direction and the line from the surface station to the grid point).

For equal values of r_s, alignment weighting causes winds at a station directly upwind or downwind of a grid point to be weighted twice as heavily as the winds for a station at right angles to the grid point.

(5) The mixed layer averaged wind at the grid point is calculated by multiplying the surface wind speed at the grid point from Step (4) by the wind speed ratio, R, at the nearest rawinsonde site. Similarly, the surface wind direction is adjusted by the wind direction factor, $\Delta\theta$.

The surface wind components in Step (4) must be computed each hour regardless of the choice of wind fields because these winds are also required in the calculation of the micrometeorological parameters described in Section 2.2.

Vertically averaged winds from the mixing height to the 850 mb, 700 mb or 500 mb levels are computed in the following manner. The 00 GMT and 12 GMT winds at each rawinsonde station are first interpolated in time, and then vertically averaged through the layer from the grid point mixing height to the selected level (e.g., 700 mb). The winds at grid point (i, j) are obtained by Equation (2-1), with the summation over rawinsonde stations instead of surface stations. Only rawinsonde stations within a 'scan-radius' of the grid point are considered. The mixing height must be lower than the pressure level that defines the top of the layer, otherwise, an error message is printed and execution of the program is terminated.

If one of the single-level upper air wind fields (e.g., 850 mb, 700 mb, or 500 mb) is chosen, only the wind data at the selected level is used to construct the wind field. For example, the 850 mb wind at each grid point is calculated by interpolating the 850 mb winds at each rawinsonde station over time, and then applying Equation (2-1) with the summation over the rawinsonde stations.

2.2 Micrometeorological Parameters

Boundary layer turbulence is generated by convective and mechanical processes. Convective or buoyancy-induced turbulence is produced by a positive (upward) heat flux at the ground which is driven by solar heating. Mechanical mixing originates from shear-induced turbulence which is caused by frictional interaction of the wind with the earth's surface. The structure of the boundary layer can be described in terms of a small number of micrometeorological variables; the surface sensible heat flux, H, the surface friction velocity, u_*, and the boundary layer height, z_i. Many studies (e.g., Deardorff and Willis 1975, van Ulden 1978) have shown the importance of these and related parameters in boundary layer meteorology. MESOPAC II uses simple empirical relationships to estimate micrometeorological parameters from routinely available meteorological measurements. Vertical dispersion and dry deposition of pollutants are parameterized in MESOPUFF II in terms of these variables. Horizontal and

near-field vertical puff growth continue to use dispersion formulas which require classification of stability into PGT classes.

The following sections describe the methods used to obtain the micrometeorological parameters needed by MESOPUFF II from routinely available meteorological data.

2.2.1 Surface Friction Velocity

The surface friction velocity, u_*, can be computed from routinely available meteorological data if the surface roughness characteristics are known. First, the sensible heat flux is calculated from an estimate of net radiation. Then u_* is determined from the wind speed, surface roughness, z_o, and heat flux.

The sensible heat flux, H, is estimated during daylight hours by the following equations (Maul 1980):

$$H = \alpha R + H_o \qquad (2\text{-}2)$$

$$R = 950 \beta \sin \upsilon \qquad (2\text{-}3)$$

$$H_o = 2.4 C - 25.5 \qquad (2\text{-}4)$$

where,

- H is the sensible heat flux (Wm^{-2}),
- H_o is the heat flux in the absence of solar incoming radiation (Wm^{-2}),
- α is a land use constant, (~ 0.3),
- R is the incoming solar radiation (Wm^{-2}),
- β is a radiation reduction factor due to the presence of clouds,
- υ is the solar elevation angle, and
- C is the opaque cloud cover (in tenths).

Table 3 contains default values for the solar radiation reduction factor (β) due to the different cloud amounts. The values of β are adapted from those used by Maul (1980).

The sine of the solar elevation angle, sin υ, is given by:

$$\sin \upsilon = \sin \phi \sin K_d + \cos \phi \cos K_d \cos H_A \tag{2-5}$$

$$H_A = (\pi/12)\ (\tau - E_m) - \lambda \tag{2-6}$$

$$E_m = 12. + 0.12357 \sin (D) - 0.004289 \cos (D) + 0.153809 \sin (2D) + 0.060783 \cos (2D) \tag{2-7}$$

$$D = (d-1)\ (360./365.242)(\pi/180) \tag{2-8}$$

$$K_D = \sin^{-1} (0.39784989 \sin (\pi\ \sigma_A/180)) \tag{2-9}$$

$$\sigma_A = 279.9348 + D(180/\pi) + 1.914827 \sin (D) - 0.079525 \cos (D) + 0.019938 \sin (2D) - 0.00162 \cos (2D) \tag{2-10}$$

where ϕ is the latitude (radians),
λ is the longitude (radians),
d is the Julian day, and
τ is the time of day (hours).

With the above estimate of H, the surface friction velocity, u_*, can be estimated during unstable conditions by the method described by Wang and Chen (1980):

$$u_* = \tilde{u}_* \{1 + a \ln [1 + b\ Q_o/\tilde{Q}_o]\} \tag{2-11}$$

$$\tilde{u}_* = \frac{k u_m}{\ln (z_m/z_o)} \tag{2-12}$$

TABLE 3. SOLAR RADIATION REDUCTION FACTOR ß

Cloud Cover (Tenths)	ß
0	1.00
1	0.91
2	0.84
3	0.79
4	0.75
5	0.72
6	0.68
7	0.62
8	0.53
9	0.41
10	0.23

$$z_m = z_{ms} - 4\, z_o \tag{2-13}$$

$$Q_o = H/(\rho\ c_p) \tag{2-14}$$

$$\tilde{Q}_o = \frac{\theta\ \tilde{u}_*^3}{k\ g\ z_m} \tag{2-15}$$

$$a = \begin{cases} 0.128 + 0.005\ \ln\ (z_o/z_m) & z_o/z_m \leq 0.01 \\ 0.107 & z_o/z_m > 0.01 \end{cases} \tag{2-16}$$

$$b = 1.95 + 32.6\ (z_o/z_m)^{0.45} \tag{2-17}$$

where,

- k is the von Karman constant ($\sim$0.4),
- c_p is the specific heat of air at constant pressure (996 $m^2/(s^2\ deg)$),
- u_* is the surface friction velocity (m/s),
- u_m is the wind speed (m/s) measured at height z_{ms} (m),
- z_o is the surface roughness (m), and
- ρ is the density of air (kg/m^3).

During stable conditions, u_* is determined by the following method (Venkatram 1980):

$$u_* = \frac{C_{DN}\ u_m}{2}\ [1 + C^{0.5}] \tag{2-18}$$

$$C_{DN} = \frac{k}{\ln\ (z_m/z_o)} \tag{2-19}$$

$$C = 1 - \frac{4\ u_o^2}{C_{DN} u_m^2} \qquad C \geq 0 \tag{2-20}$$

$$u_o^2 = \frac{\gamma\ z_m}{k\ A} \tag{2-21}$$

where γ and A are constants with values of 4.7 and 1100, respectively, and C_{DN} is the neutral drag coefficient.

2.2.2 Monin-Obukhov Length

The Monin-Obukhov length, L, is defined as:

$$L \equiv - \frac{u_*^3 T_o}{g\ k\ Q_o} \tag{2-22}$$

where T_o is the observed air temperature and g in the acceleration due to gravity. During unstable conditions, L is calculated directly from its definition using values of u_* and Q_o derived earlier. During stable conditions, L is given by Venkatram (1980b) as:

$$L = 1100\ u_*^2 \tag{2-23}$$

2.2.3 Mixed Layer Height

During daylight hours, solar radiation reaching the ground produces a positive (upward) flux of sensible heat and the development of a well-mixed adiabatic layer. If the hourly variation of H is known, the mixed layer height, z_i, at time t + 1 can be estimated from z_i at time t in a stepwise manner (Maul 1980).

$$(z_i)_{t+1} = \left[(z_i)^2_t + \frac{2H(1+E)\Delta t}{\psi_1 \rho c_p} - \frac{2(\Delta\theta)_t (z_i)_t}{\psi_1} \right]^{1/2} + \frac{(\Delta\theta)_{t+1}}{\psi_1} \qquad (2\text{-}24)$$

$$(\Delta\theta)_{t+1} = \left(\frac{2\psi_1 EH\Delta t}{\rho c_p} \right)^{1/2} \qquad (2\text{-}25)$$

where

ψ_1 is the potential temperature lapse rate in the layer above z_i,

Δt is the time step (3600 s),

E is a constant (~0.15), and

$\Delta\theta$ is the temperature discontinuity at the top of the mixed layer.

The lapse rate, ψ_1, is determined through a layer Δz meters above the previous hour's convective mixing height. For daytime hours up to 23 GMT, the morning (12 GMT) sounding at the nearest rawinsonde station is used to calculate ψ_1. After 23 GMT, the evening (00 GMT) sounding is used. To avoid computational problems, ψ_1 is not allowed to be less than 0.001 °K/m.

The neutral (shear produced) boundary layer height is given by Venkatram (1980) as:

$$z_i = \frac{B\ u_*}{(fN_B)^{1/2}} \qquad (2\text{-}26)$$

where f is the Coriolis parameter,

B is a constant ($\sqrt{2}$), and

N_B is the Brunt-Vaisala frequency in the stable layer aloft.

The daytime mixing height is the maximum of the convective and mechanical values predicted by Equations 2-25 and 2-26.

In the stable boundary layer, mechanical turbulence production determines the vertical extent of dispersion. Venkatram (1980b) provides the following empirical relationship to estimate z_i during stable conditions.

$$z_i = 2400\ u_*^{3/2} \qquad (2\text{-}27)$$

2.2.4 Convective Velocity Scale

During convective conditions, turbulence is generated primarily by the sensible heat flux originating from the ground. The appropriate velocity scale during these conditions is the convective velocity, w_*.

$$w_* \equiv \left(\frac{g}{T_o} Q_o\ z_i\right)^{1/3} \qquad (2\text{-}28)$$

The convective velocity can be calculated directly from its definition, since Q_o and z_i have been determined from Equations 2-14 and 2-24, respectively.

2.3 Dry Deposition - Three-Layer Model

The rate at which pollutants are deposited at the surface depends on many factors: the state of the atmosphere, the characteristics of the surface, and the properties of the pollutant. For example, the rate of deposition can sometimes be limited by the rate of pollutant transfer to the surface by atmospheric diffusion processes. Due to the importance of vegetation as a sink for atmospheric pollutants, the structure of the canopy and the physiological state of the vegetation are also important factors. The properties of a pollutant such as its solubility, molecular diffusivity and for larger particles, the size and shape of the particles are additional factors that influence the rate of deposition. Table 4 contains a listing

TABLE 4. FACTORS INFLUENCING DRY DEPOSITION REMOVAL RATES

Micrometeorology variables	Depositing Material		Surface Variables
	Particles	Gases	
Aerodynamic roughness:	Agglomeration	Chemical activity	Accommodation:
-Mass transfer	Diameter	Diffusion:	-Exudates
(a) Particles	Density	-Brownian	-Trichomes
(b) Gases	Diffusion:	-Eddy	-Pubescence
-Heat	-Brownian	Partial pressure in equilibrium with surface	-Wax
-Momentum	-Eddy equal to	Solubility	Biotic surfaces
Atmospheric stability	(a) Particle		Canopy growth:
Diffusion, effect of:	(b) Momentum		-Dormant
-Canopy	(c) Heat		-Expanding
-Diurnal variation	-Effect of canopy on		Senescent
-Fetch	Diffusiophoresis		Canopy Structure:
Flow separation:	Electrostatic effects:		-Areal density
-Above canopy	-Attraction		-Bark
-Below canopy	-Repulsion		-Bole
Friction velocity	Gravitational settling		-Leaves
Inversion layer	Hydroscopicity		-Porosity
Pollutant concentration	Impaction		-Reproductive structure
Relative humidity	Interception		-Soils
Seasonal variation	Momentum		-Stem
Solar radiation	Physical properties		-Type
Surface heating	Resuspension		Electrostatic properties
Temperature	Shape		Leaf-vegetation:
Terrain:	Size		-Boundary Layer
-Uniform	Solubility		-Change at high winds
-Nonuniform	Thermophoresis		-Flutter
Turbulence			-Stomatal resistance
Wind velocity			Non-biotic surfaces
Zero-plane displacements:			pH effects on:
-Mass transfer			-Reaction
(a) Particles			-Solubility
(b) Gases			Pollutant penetration and distribution in canopy
-Heat			Prior deposition loading
-Momentum			Water

From: Sehmel (1980)

compiled by Sehmel (1980) of the variables believed to be most important in influencing dry deposition rates.

The dry flux of a pollutant can be written (Slinn et al. 1978) as:

$$F_d = F_z + v_g C \qquad (2\text{-}29)$$

where

F_d is the total (downward) dry flux,
F_z is the turbulent and molecular diffusive flux,
v_g is the average drift velocity due to gravitational settling and phoretic effects, and
C is the pollutant concentration.

For larger particles (diameters >1 μm), gravitational settling and particle inertia become increasingly important effects. Brownian diffusion dominates the mass transfer of gases and small particles (diameters <0.1 μm) in the near surface quasi-laminar layer. As shown in Figure 3, a minimum in deposition velocity is observed from particles in the range 0.1-1.0 μm where these mechanism are less effective (Hicks 1982). Most models of dry deposition use the concept of a deposition velocity (Chamberlain and Chadwick 1953) to express the total dry flux:

$$F_d = v_d C \qquad (2\text{-}30)$$

where v_d is the deposition velocity (including both gravitational and diffusive effects) at a reference height.

Due to the number and variability of the factors influencing deposition rates, reported deposition velocities exhibit considerable variability. For example, SO_2 deposition velocities summarized by Sehmel (1980) range over two orders of magnitude (Figure 4). Although it is not possible to include the effects of all the variables listed in Table 4 in determining v_d, it is possible to improve upon the assumption commonly used in mesoscale models

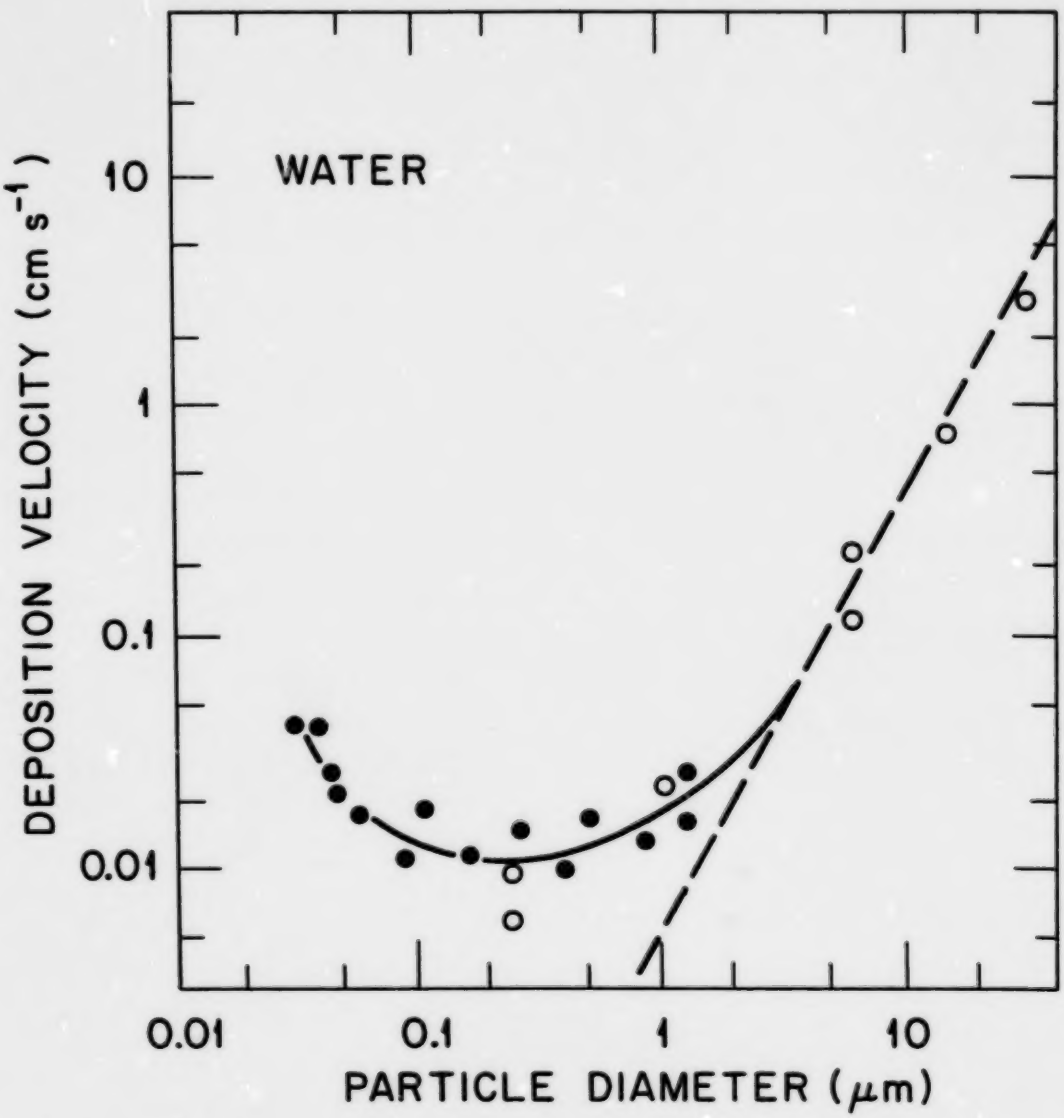

Figure 3 Particle Deposition to Water Surfaces. Solid Circles are Due to Moller and Schumann (1979), Open Circles to Sehmel and Sutter (1973). The Dashed Line at the Right Represents the Terminal Settling Speed for 1.5 g cm^{-3} Particles. Source: Hicks (1982)

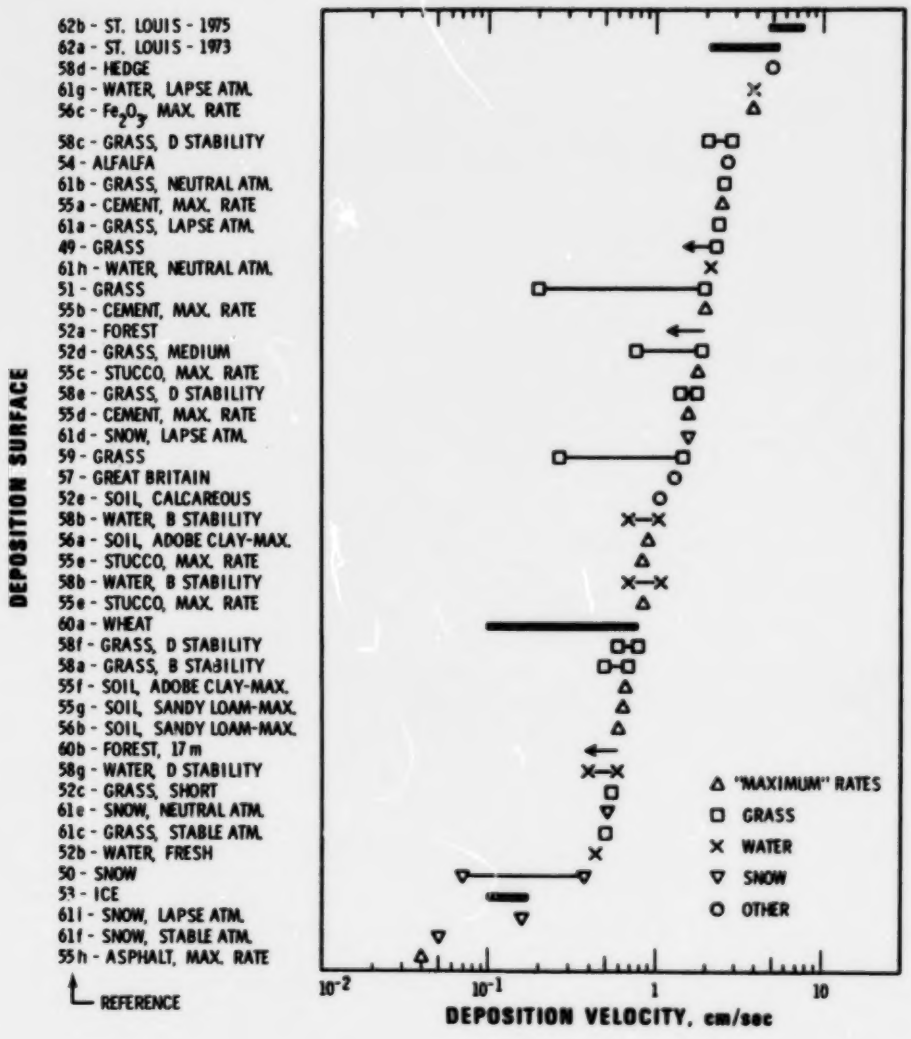

Figure 4 SO_2 Deposition Velocities
Source: Sehmel (1980)

of spatially and temporally constant deposition velocities. In MESOPUFF II, the deposition velocity is expressed as the inverse of a sum of resistances to transfer of the pollutant through the atmosphere to the surface.

$$v_d = (r_a + r_s + r_c)^{-1} \tag{2-31}$$

where r_a is the aerodynamic resistance (s/m),
r_s is the surface resistance (s/m), and
r_c is the canopy resistance (s/m).

The aerodynamic resistance is the resistance to pollutant transfer through the atmospheric surface layer. It is a function of wind speed, atmospheric stability, and surface roughness. Except for very large particles, the aerodynamic resistance for gases and particles is the same. The surface resistance represents the resistance to transfer across the quasi-laminar layer surrounding smooth surfaces. Wind tunnel studies have shown that the thickness of this layer is typically about 50 μm (Hicks 1982). However, surface roughness elements can sometimes penetrate this layer, providing an alternative route for the transfer. Therefore, r_a is an average value of this resistance. The canopy resistance is the resistance to transfer within the surface or plant constituting the final resting place for the pollutant. The canopy resistance depends on the characteristics of the pollutant (e.g., solubility) as well as the physiological properties of the vegetation.

The aerodynamic resistance, r_a, is given by Wesely and Hicks (1977) as:

$$r_a = (k\, u_*)^{-1} [\ln(z_s/z_o) - \psi_H] \tag{2-32}$$

$$\psi_H = \begin{cases} -5z_s/L & 0 < z_s/L < 1 \\ \exp [0.598 + 0.39 \ln (-z_s/L) - 0.090 \{\ln(-z_s/L)\}^2] & -1 < z_s/L < 0 \end{cases} \tag{2-33}$$

where z_s is the reference height (10 meters in MESOPUFF II),

z_o is the surface roughness length (m),

u_* is the friction velocity (m/s),

Ψ_H is a function accounting for stability effects,

k is the von Karman constant, and

L is Monin-Obukhov length (m).

The surface resistance, r_s, can be expressed (Wesely and Hicks 1977) as:

$$r_s = (k\, u_*)^{-1}\, kB^{-1} \qquad (2\text{-}34)$$

where B^{-1} is the surface transfer coefficient.

For SO_2, $kB^{-1} \approx 2.6$ (Wesely and Hicks 1977). The other gaseous pollutants in MESOPUFF II (e.g., NO_x, HNO_3) are assumed to have similar values of kB^{-1}. For particles, r_s is a complex function of many factors. Depending upon the pollutant size distribution, particle inertia and gravitational settling effects may be important. Given current uncertainties regarding r_s for particles, r_s is simply assumed constant for $SO_4^=$ and NO_3^- with a default value of 10 s/cm. Although Wesely and Hicks (1977) suggest r_s may be as low as 1 s/cm, the larger value is presently used in the model to be consistent with deposition velocities of $\sim$0.1 cm/s found in other studies (e.g., Garland 1978) for sulfate.

Shieh et al. (1979) estimate canopy resistance for SO_2 as a function of land use and stability class for summertime conditions. These values, contained in Table 5, are used as default values in MESOPUFF II. It should be noted that these values are based only on expected midsummer conditions. More appropriate values (e.g., for snow covered surfaces) may be entered for model applications during other seasons.

Based upon its high solubility and reactivity, r_c for HNO_3 is assumed equal to zero (Hicks 1982). Canopy resistance for NO_x are

TABLE 5. SUMMERTIME SO_2 CANOPY RESISTANCES AS A FUNCTION OF LAND USE TYPE AND STABILITY CLASS

Category	Land Use Type	z_o (m)	Stability Class A,B,C	D	E	F
1	cropland and pasture	0.20	100.	300.	1000.	0.
2	cropland, woodland and grazing land	0.30	100.	300.	1000.	0.
3	irrigated crops	0.05	100.	300.	1000.	0.
4	grazed forest and woodland	0.90	100.	300.	1000.	0.
5	ungrazed forest and woodland	1.00	100.	300.	1000.	0.
6	subhumid grassland and semiarid grazing land	0.10	100.	300.	1000.	0.
7	open woodland grazed	0.20	100.	300.	1000.	0.
8	desert shrubland	0.30	200.	500.	1000.	1000.
9	swamp	0.20	50.	75.	100.	0.
10	marshland	0.50	75.	300.	1000.	0.
11	metropolitan city	1.00	1000.	1000.	1000.	0.
12	lake or ocean	10^{-4}	0.	0.	0.	0.

From: Shieh, Wesely, and Hicks (1979).

1.3 s/cm (A-C stability), 5 s/cm (D stability), and 15 s/cm (E-F stability). Uptake of the particles $SO_4^=$ and NO_3^- by plant stomata is less relevant; therefore, total resistance for $SO_4^=$ and NO_3^- is determined by r_a and r_s (i.e., $r_c = 0$).

With knowledge of the concentration and the deposition velocity, the pollutant flux is determined by Equation 2-30. MESOPUFF II has two options for treating the removal of pollutant from a puff. The first option is the commonly used source depletion approximation. This method assumes that material deposited is removed from the full depth of the puff. The change in mass is:

$$Q(t+1) = Q(t) \exp\left[- \frac{v_d \ \Delta t}{\Delta s} \int_s^{s + \Delta s} g(s') \, ds' \right] \qquad (2\text{-}35)$$

Where $Q(t)$, $Q(t+1)$ is the mass (g) of pollutant in the puff at the beginning and end of the time step,

s, $s + \Delta s$ is the position of the puff at the beginning and end of the time step, and

$g(s)$ is the vertical term of the Gaussian puff equation as given by Equation 2-59. For a puff uniformly mixed in the vertical, $g(s) = 1/z_i$.

The source depletion model effectively enhances the rate of vertical diffusion of the pollutant because mass removed at the surface is immediately replaced with material from above. However, in the atmosphere, the rate of deposition can be limited (usually only during stable conditions) by the rate of pollutant mass transfer through the boundary layer to the surface layer. This overall boundary layer resistance is not included in the aerodynamic resistance. Horst (1977) suggests that the source depletion model may introduce a bias in the deposition flux. Excessively high deposition fluxes and concentrations may be predicted by the source depletion model in the near-field, and as a result, the concentrations and deposition fluxes may be underpredicted further

downwind. This effect is illustrated in Figure 5 where the source depletion model results are compared to those of the surface depletion model of Horst (1977).

To account for the effect of boundary layer mixing, MESOPUFF II has the option to treat puffs that have become vertically well-mixed with a 3-layer model (see Figure 6). The surface layer is a shallow layer (10 m) next to the ground that rapidly adjusts to changes in surface conditions. Pollutants in the middle layer are uniformly mixed up to the top of the current boundary layer. The upper layer consists of pollutant material above the boundary layer dispersed upward during previous turbulent activity. The pollutant flux into the surface layer is:

$$\text{Flux} = \kappa \, (C_m - C_s) \, / \, (z_i - z_s) = v_d \, C_s \qquad (2\text{-}36)$$

where κ is an overall boundary layer eddy diffusivity (m^2/s),
C_m is the concentration in the middle layer, and
C_s is the concentration at the top of the surface layer.

During stable conditions, κ is given by Brost and Wyngaard (1978) as:

$$\kappa = k_1 \, u_* \, z_i \qquad (2\text{-}37)$$

and during neutral or unstable conditions κ is:

$$\kappa = \text{Maximum} \{k_1 \, u_* \, z_i, \; k_2 \, w_* \, z_i\} \qquad (2\text{-}38)$$

The constants k_1 and k_2 have default values of 0.01 and 0.1, respectively.

The term $v_d \, C_s$ can be written as $v_d' \, C_m$, where v_d' is an effective deposition velocity taking into account boundary layer mass transfer.

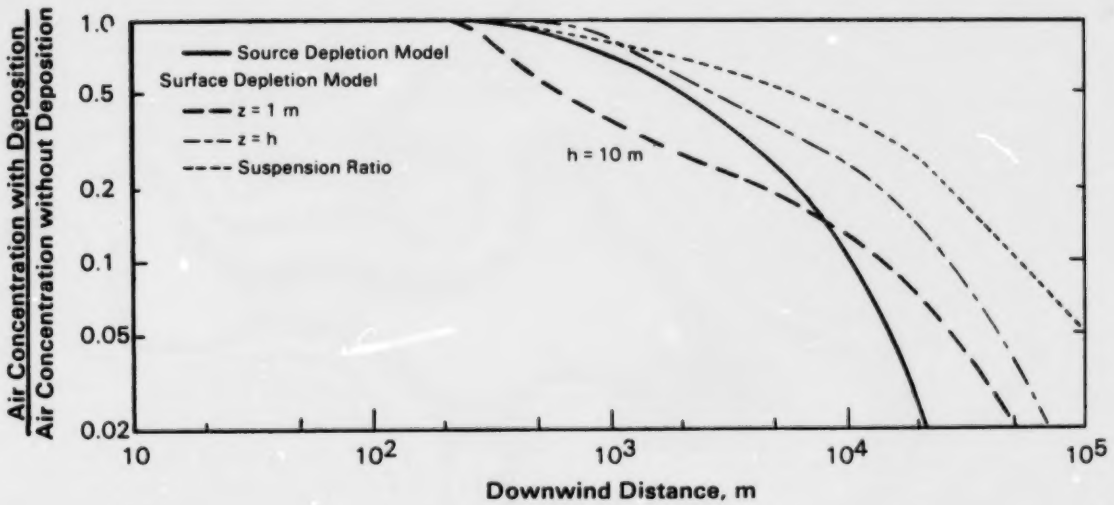

Figure 5 Comparison of Source Depletion and Surface Depletion Models. For $v_d/u = 10^{-2}$, Stable Thermal Stratification (F Stability) from Horst (1977)

8304089

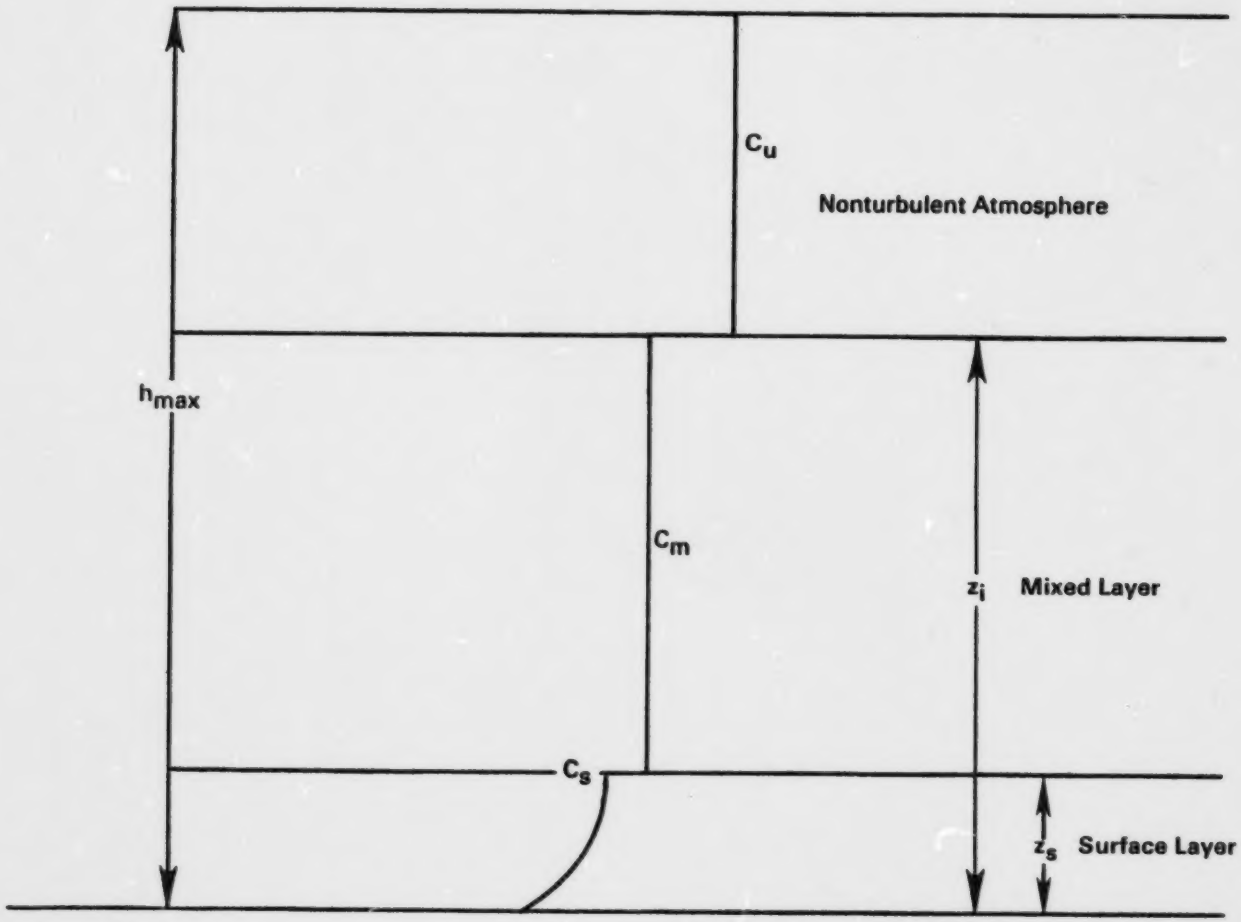

Figure 6 Optional Three Layer System Used in MESOPUFF II

$$v_d' = \frac{\kappa\, v_d}{\kappa + v_d(z_i - z_s)} \qquad (2\text{-}39)$$

In the 3-layer model, only material in the surface layer is available for deposition at the surface. The effective deposition velocity, v_d' is used to evaluate the change in pollutant mass in the puff due to dry deposition. The model predictions are those corresponding to C_s in Figure 6.

2.4 Chemical Transformations

The accuracy of air quality models for chemically reactive species depends strongly on the chemical submodel, as well as the transport, diffusion, and deposition formulations. The fidelity of atmospheric chemical mechanisms is often limited by the availability of kinetic and mechanistic data for the species of concern and sometimes the model's structure. For example, often the atmospheric chemistry of emitted compounds depends on numerous other compounds formed and destroyed in other chemical reactions. Not only are the rate constants and products uncertain for many of these reactions, but also the model's formulation may not allow for inclusion of intermediate species and/or second-order reactions. The latter is true for the puff transport/dispersion formulation used in the MESOPUFF II model. Thus, chemical mechanisms for models such as MESOPUFF II must be formulated as pseudo-first-order reactions. The accuracy of the first-order reaction mechanism may be enhanced by parameterization of the rate constants so as to reflect the characteristics of the higher-order reaction system.

The chemical process of concern for the MESOPUFF II model are the conversions of sulfur dioxide (SO_2) to sulfate aerosol ($SO_4^=$) and oxides of nitrogen (NO_x) to nitrate aerosol (NO_3^-). Although the atmospheric chemistry of these compounds has been studied for nearly two decades, substantial uncertainties exist in the current chemical knowledge of SO_x and NO_x reaction pathways and rates under ambient conditions.

Laboratory and field studies have shown that chemical transformation rates for these species can vary several orders of magnitude under different environmental conditions (Calvert et al. 1978; Wilson 1981; Richards et al. 1981; Newman 1981). It is, therefore, important for the chemical submodel to incorporate the dependency of transformation rates on environmental conditions.

A first order reaction mechanism consisting of the following reactions has been formulated for MESOPUFF II:

$$SO_2 \rightarrow SO_4^{=} \qquad (2\text{-}40)$$

$$NO_x \rightarrow HNO_3 \qquad (2\text{-}41)$$

$$NO_x \rightarrow RNO_3 \qquad (2\text{-}42)$$

$$HNO_3 \overset{NH_3}{\rightleftharpoons} NO_3^- \qquad (2\text{-}43)$$

The rate constants have been parameterized in terms of environmental conditions such as solar radiation, relative humidity, temperature, and background ozone concentrations. The parameterizations have been developed from laboratory data, field data, and analysis of nonlinear chemical mechanisms for SO_x and NO_x oxidation. The following subsections describe the rationale for and development of the MESOPUFF II chemical transformation scheme.

2.4.1 Chemical Pathways for Sulfate and Nitrate Aerosol Formation

Research performed during the last twenty years has identified many of the important pathways for SO_2 and NO_x oxidation. Laboratory and field studies have shown fine particulate matter to be a major product of SO_2 oxidation and a minor product of NO_x oxidation under ambient conditions. Figures 7 and 8 illustrate the chemical pathways for SO_2 and NO_x oxidation, and aerosol formation. Oxidation may occur by gas and aqueous

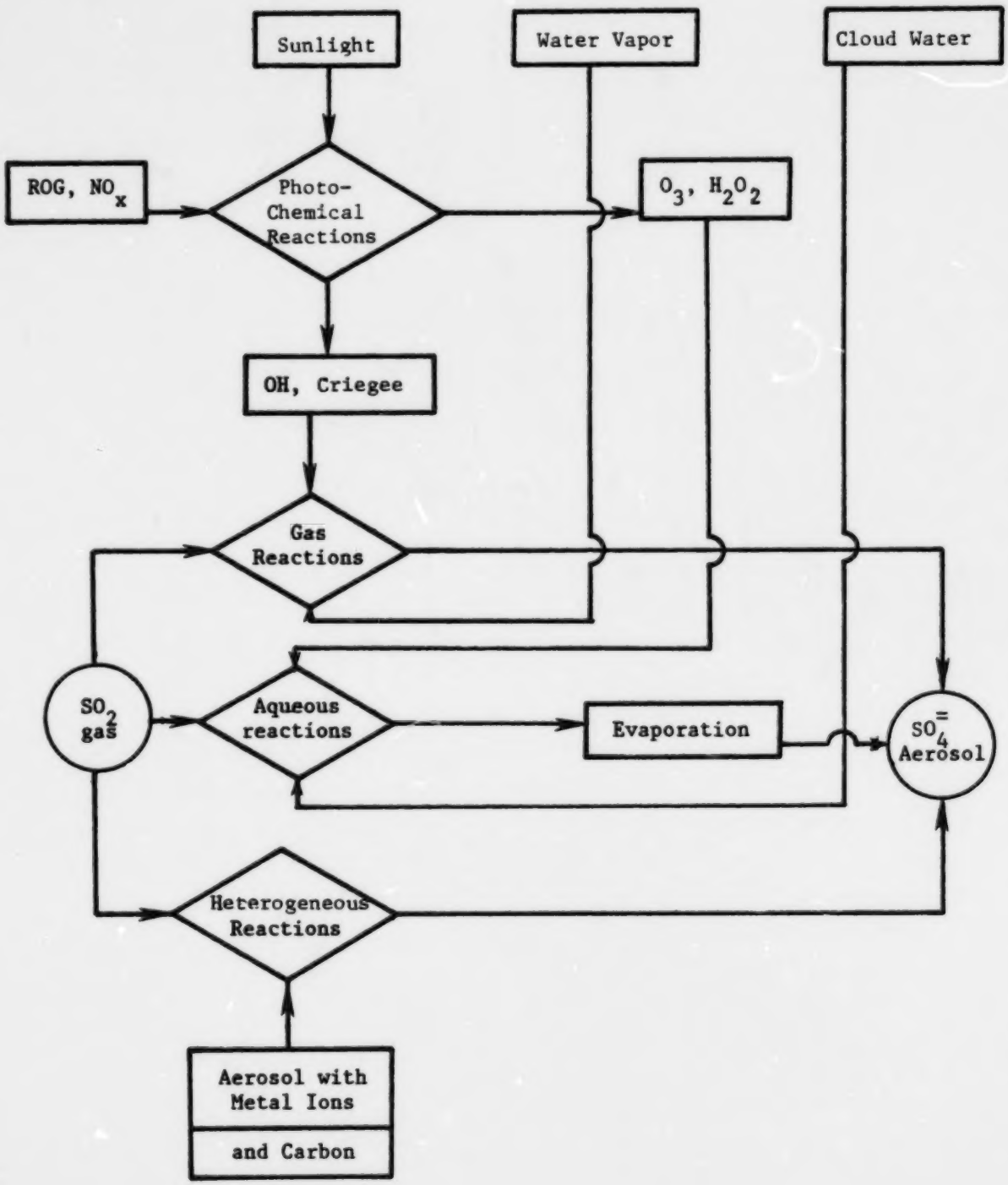

Figure 7 SO_2 Oxidation Pathways

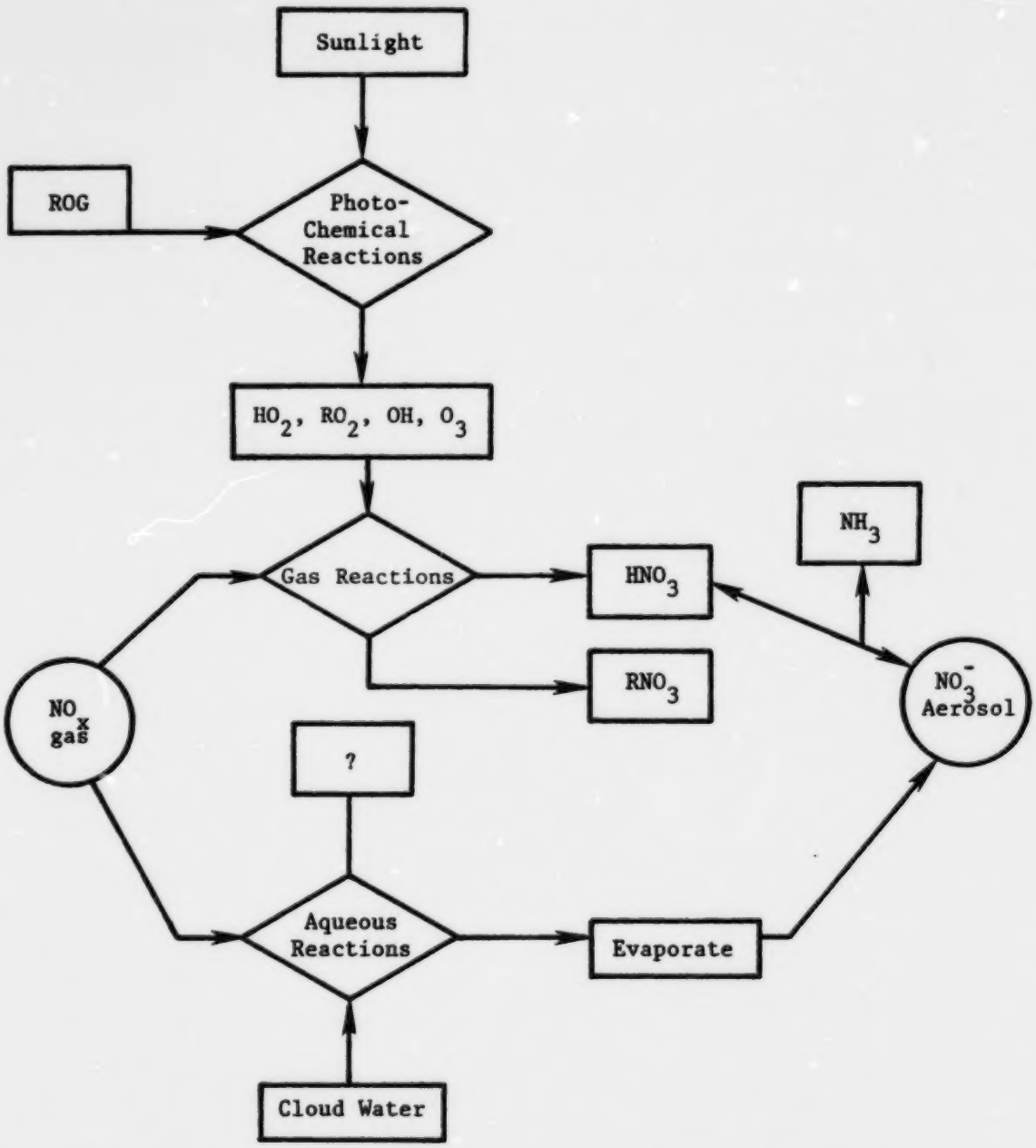

Figure 8 NO_x Oxidation Pathways

phase reactions. The gas phase reactions for both SO_x and NO_x involve free radical photochemistry and, thus, are coupled to the oxidation of reactive organic gases (ROG). The aqueous phase oxidation reactions for SO_x and NO_x are less well understood than the gas phase reactions, however, photochemical products such as ozone (O_3) and hydrogen peroxide (H_2O_2) are believed to be the principal oxidants for SO_2.

Homogenous gas phase reactions are believed to be the dominant SO_2 oxidation pathway in the presence of sunlight and absence of clouds or fog (Calvert et al. 1978). Three of the most important reactions for SO_2 are:

$$SO_2 + OH + M \rightarrow HSO_3 + M \qquad (2\text{-}44)$$

$$SO_2 + CH_2O_2 \rightarrow SO_3 + CH_2O \qquad (2\text{-}45)$$

$$SO_2 + CH_3CHOO \rightarrow SO_3 + CH_3CHO \qquad (2\text{-}46)$$

In the presence of trace amounts of water vapor, HSO_3 and SO_3 rapidly form a sulfate aerosol or attach to pre-existing aerosols. Reactions of HSO_3 with NO in the presence of O_2 may occur but the mechanism remains uncertain (Calvert et al. 1978). The reaction with the hydroxyl radical (OH) is believed to be most important. The reactions with the Criegee biradicals, formed from ozone-alkene reactions, may be important at high alkene concentrations in urban environments (Atkinson and Lloyd 1980). These reactions can produce SO_2 oxidation rates of up to 5% per hour.

SO_2 oxidation may also occur via reactions of the dissolved S(IV) constituents, primarily bisulfate and sulfite, with dissolved ozone and hydrogen peroxide (H_2O_2) (Maahs 1982; Penkett et al. 1979). The aqueous phase oxidation may also be catalyzed by Mn^{++}, Fe^{++}, and/or elemental carbon (Martin 1982). Recent reviews suggest that oxidation by H_2O_2 may be the dominant process under acidic conditions (Schwartz 1982). Although there is considerable uncertainty whether H_2O_2 production in the gas or aqueous phase is sufficient to sustain this reaction, relatively small amounts of H_2O_2 can produce transformation rates of up to 100% per hour

locally in cloud or rain water. Since cloud water is believed to be recycled (condensed-evaporated) rapidly, the aqueous phase reactions may be an important pathway for sulfate aerosol formation under cloudy or foggy conditions (Hegg and Hobbs 1981).

The oxidation of NO_x is strongly dependent on gas phase $ROG/NO_x/O_3$ photochemistry and is generally more rapid than SO_2 oxidation. As shown in Figure 8, NO_x can be oxidized to nitric acid (HNO_3) and organic nitrates (RNO_3) including oxygenated nitrates such as peroxyacetylnitrate (PAN). Nitric acid formation occurs primarily by the reaction of NO_2 with OH (at a rate ~8 times faster than SO_2 + OH). Oxidation of NO_x to N_2O_5 (with involvement of O_3) followed by a heterogeneous reaction with water and reactions of NO_3 with aromatic hydrocarbons may also lead to HNO_3 formation. HNO_3 is, in turn, destroyed very slowly by photolysis and reaction with OH.

Nitric acid combines with ammonia gas to form solid or aqueous ammonium nitrate (NH_4NO_3). Unlike $SO_4^=$ formation, the NO_3^- formation process is reversible. Equilibrium is established between nitric acid, ammonia, and ammonium nitrate:

$$NH_4NO_3\ (s \text{ or } aq) \underset{}{\overset{K_H}{\rightleftharpoons}} HNO_3(g) + NH_3(g) \qquad (2\text{-}47)$$

The equilibrium constant

$$K_H = \frac{[NH_3]\ [HNO_3]}{[NH_4NO_3]} \qquad (2\text{-}48)$$

is dependent on temperature and relative humidity in a nonlinear manner as shown in Figure 9 (Stelson and Seinfeld 1982). The equilibrium constant can vary several orders of magnitude over a typical diurnal cycle. Given fixed amounts of total nitrate, ammonia, and water vapor, higher NH_4NO_3 concentrations are expected at night, due to lower nighttime temperature and

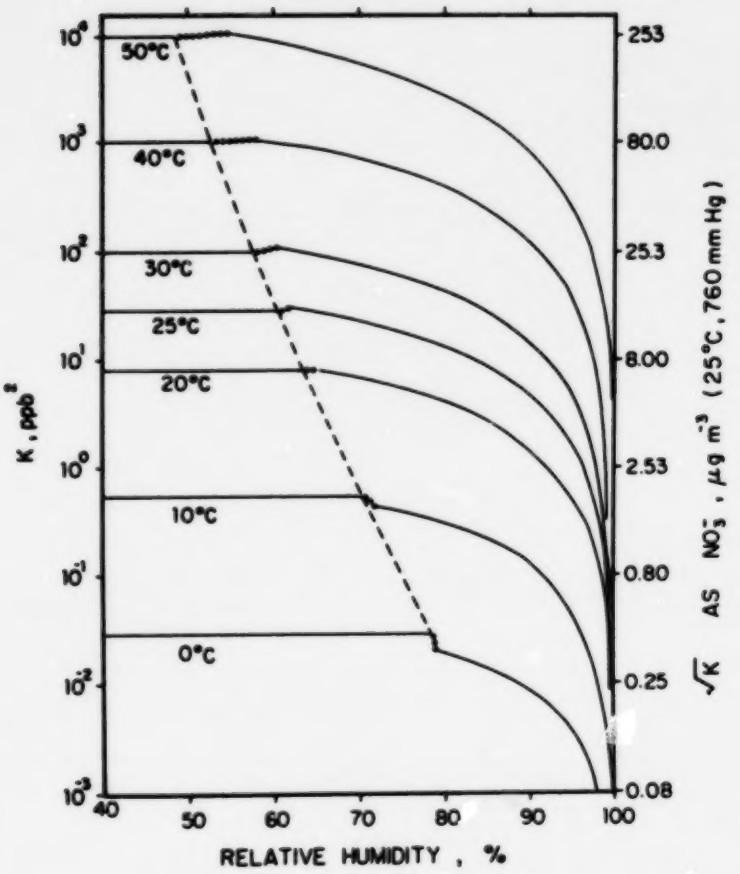

Figure 9 NH_4NO_3 Dissociation Constant Temperature and Relative Humidity Dependence
Source: Stelson and Seinfeld (1982)

higher relative humidity. Thus, the nitrate aerosol cannot be considered a stable product like sulfate. Also, unlike $SO_4^=$, its ambient concentrations are limited by the availability of ammonia which is preferentially scavenged by sulfate (Stelson et al. 1983).

The formation of organic nitrate such as peroxyacetylnitrate (PAN) and PAN analogs is the second major pathway for NO_x oxidation. The organic nitrates are formed primarily by reactions of NO_2 with RCO_3 radicals (such as acetylperoxy). Organic nitrates may also be formed by reactions of NO with RO_2 radicals and NO_2 with RO radicals. The RCO_3 radicals are formed from acetaldehyde and higher aldehydes which are emitted directly by sources and photochemically formed from organic gases. PAN formation rates are, therefore, strongly dependent on hydrocarbon loadings. The stability of PAN, and therefore, its net formation rate, strongly depends on temperature. PAN decomposes into NO_2 and RCO_3 at a rate which increases with temperature. This has lead many scientists to view PAN as more of a temporary reservoir for NO_2 than a permanent sink. The results of multi-day simulations of $HC/NO_x/O_3$ systems with diurnally varying temperature and radiation performed at ERT suggest the cumulative formation of PAN greatly exceeds its decomposition, hence we believe PAN is a major NO_x sink. However, in contrast to the HNO_3 pathway, there is no evidence of nitrate aerosol formation from PAN.

Little is known regarding aqueous phase oxidation of dissolved NO_2 to NO_3^-. NO_2 has low solubility and at this time the only reaction of importance involves S(IV)aq + N(III)aq (Schwartz and White 1982; Martin et al. 1981). Its reaction products are unknown. Based on the current information, the aqueous phase oxidation pathways appears to be far less important than the gas phase oxidation pathway for NO_x.

2.4.2 Development of a Pseudo-First Order Reaction Mechanism

Rate constant expressions for reactions 1-3 (Equations 2-40 to 2-42) were developed to represent SO_2 and NO_x oxidation under different environmental conditions. The gas and aqueous components of the SO_2

oxidation rate were developed separately. Only gas phase oxidation was considered for NO_x. The $HNO_3/NH_3/NH_4NO_3$ equilibrium relationship (Equation 2-43) was incorporated directly into the mechanism. Since the gas phase chemistry for SO_2 and NO_x is better understood than the aqueous phase, greater emphasis was placed on developing the gas component of the psuedo-first order rate expressions.

Since the oxidation of SO_2 and NO_x depends strongly on gas phase photochemistry, rate expressions were derived from the results of photochemical model simulations. A variable volume Lagrangian photochemical box model was exercised over a wide range of environmental conditions. The model was designed to simulate plume gases dispersing into and reacting with background air. The Atkinson et al. (1982) photochemical mechanism was employed for the calculations. It incorporates the important gas phase reaction pathways for the $ROG/NO_x/SO_x$ chemical system shown in Appendix A.

Five groups of parameters expected to influence photooxidation rates of plume gases were allowed to vary in the photochemical model runs. These surrogate parameters included season, background reactivity, dispersion conditions, time of emissions release, and plume NO_x loadings. A total of 144 model runs were made representing parameter combinations for 3 different seasons, 4 different background reactivities, 2 different dispersion conditions, 2 different times of emissions release, and 3 different plume NO_x loadings.

Solar radiation and ambient temperature data for the photochemical model runs varied with season. Diurnally varying clear sky solar radiation for a latitude of 40° and daily average temperatures of 30, 20 and 10°C were employed for the summer, fall, and winter seasons, respectively. The background air concentrations included 11 classes of ROG compounds and ozone. The background ROG concentrations of 0.05, 0.25, 0.50, 2.0 ppmC were employed. The composition of ROG was assumed to be 60% reactive alkanes, 10% alkenes, 25% aromatics, and 5% aldehydes on a carbon basis in all cases. Background ozone concentrations were varied between 0.02 and

0.20 ppm. Plume NO_x loadings were varied from 0.007 to 1.4 ppm. Relative humidity of 60% and a constant initial SO_2 concentration of 2.0 ppm were employed for all the calculations. All parameter values used for the simulation are summarized in Table 6.

The runs generated a data base with 1224 hourly conversion rates and associated environmental conditions. The data base included the conversion rate of SO_2 to $SO_4^=$, NO_x to all products and NO_x to nitric acid. The solar radiation and concentrations of NO_x, ROG, and O_3 at the midpoint of the hour were stored along with the time, temperature, stability, release time, etc. for each hour.

Stepwise linear regression on the logarithms of the output variables was performed to determine the controlling variables and the best regression equations. Solar radiation, background ozone concentrations, and atmospheric stability were found to be important parameters controlling daylight gas phase SO_2 oxidation rates. Background ozone concentration, atmospheric stability, and NO_x concentrations were found to be most highly correlated with the predicted NO_x oxidation rates. The following hourly transformation rate expressions were determined:

$$k_{1G} = 36\ R^{0.55} OZ^{0.71} S^{-1.29} \quad \text{(gas component)} \tag{2-49}$$

$$k_2 = 1206\ OZ^{1.50}\ S^{-1.41} NOX^{-0.33} \tag{2-50}$$

$$k_3 = 1261\ OZ^{1.45}\ S^{-1.34}\ NOX^{-0.12} \tag{2-51}$$

where k_{1G} is SO_2 to $SO_4^=$ transformation rate (% per hour);
k_2 is NO_x to HNO_3 + RNO_3 transformation rate (% per hour)*;
k_3 is NO_x to HNO_3 (only) transformation rate (% per hour);

*The rate constant for NO_x → RNO_3 is k_2-k_3.

TABLE 6. PARAMETER VARIATIONS IN THE PHOTOCHEMICAL MODELING SIMULATIONS

Surrogate Parameter	Number of Variations	Model Input Parameters and Variations
Season	3	Ambient temperature and solar radiation varied with season. Ambient temperatures of 30, 20, and 10°C were employed for the summer, fall, and winter cases, respectively. Diurnally varying clear sky solar radiation for 40° latitude in the 3 seasons were employed.
Background Air Reactivity	4	Background air concentrations of ozone and ROG were varied together to represent background air reactivity. Background ozone concentrations were assumed to be correlated with season. Ozone concentrations of 0.02, 0.05, 0.08, and 0.20 ppm were employed for summer. Fall and winter ozone concentrations equal to 75 and 50% of the summer values were employed. The corresponding four ROG concentrations employed were 0.05, 0.25, 0.50, and 2.0 ppmC. The composition of the ROG was assumed to be 60% reactive alkanes, 10% alkenes, 25% aromatics, and 5% aldehydes.
Dispersion	2	The rate of plume dilution varied with atmospheric stability and wind speed. A stable case with 1.5 m/sec wind speed and a slightly unstable case with 5 m/sec wind speed were assumed. Dilution rates were based on the time rate of change of plume cross-sectional area ($\sigma_y\sigma_z$) from an initial area of 10,000 m^2.
Release Time	2	Sunrise and noon time were used as emission release times.
Plume NO_x Loading	3	Initial (at $\sigma_y\sigma_z = 10^4 m^2$) plume NO_x concentrations of 0.007, 0.35, and 1.40 ppm were employed. The NO_x was partitioned as 90% NO and 10% NO_2 on a volume basis.

R is total solar radiation (kwatt/m^2);

OZ is background ozone concentration (ppm);

S is atmospheric stability index ranging from 2 to 6 (e.g., 2 for PGT stability classes A and B, 4 for class D, and 6 for class F);

NO_x is ambient NO_x concentration (ppm), minimum value is 10^{-4}ppm.

The correlation coefficients (R^2) for these regression equations are 0.80, 0.89, and 0.87, respectively, which indicate good correlations.

The dependency of these transformation expressions on environmental parameters is consistent with physical expectations. The rates are inversely proportional to the stability index which is consistent with the expectation that higher background air entrainment rates (i.e., low stability index) should result in higher conversion rates. They are proportional to the background ozone concentration. Since ozone can be thought of as a surrogate for OH concentration, this is consistent with expectations from the gas phase chemistry. The SO_2 rate expression is also dependent on solar radiation. Since the rate of the photolytic reactions, which generate the free radicals, depend directly on the radiation intensity, this result is expected. The NO_x expression has a weak inverse dependence on the NO_x concentration which is consistent with the expectation that higher NO_x concentration impedes oxidation rates. A similar dependence was expected for the SO_2 oxidation rates. However, the statistical analysis indicated NO_x concentration was not nearly as significant as the three other parameters in the SO_2 rate expression.

An aqueous phase SO_2 conversion rate expression was determined empirically. Since the amount of aqueous phase S(IV) available for conversion depends on the amount of water present (as well as condensation/evaporation rates and SO_2 solubility which in turn depends on pH, etc.), relative humidity was selected as a commonly available surrogate for liquid water content. Although conversion may occur rapidly in the aqueous phase, only a small portion of the SO_2 is in the aqueous phase. For this reason, a relatively low maximum aqueous oxidation rate (to be applied to SO_2(g)) was selected: three percent per hour. Since observations of $SO_2/SO_4^=$

in plumes suggest overall oxidation rates increase dramatically at high relative humidity (Gillani et al. 1981) a higher order dependence on humidity was selected. The aqueous phase component of k_1 is

$$k_{1A} = 3x10^{-8}RH^4 \text{ (aqueous component)*} \quad (2\text{-}52)$$

where RH is the relative humidity (in percent). A minimum of 0.2% per hour is used for k_{1A}. The accuracy of this expression is highly uncertain. Depending on environmental conditions, such as the availability of hydrogen peroxide or metal catalysts, the actual conversion rate may be an order of magnitude higher or lower than indicated by the expression.

Other researchers have formulated SO_2 oxidation rate expressions based on observations. Henry and Hidy (1981, 1982) employed principal component analysis of urban aerometric data to derive expressions for the homogeneous and heterogeneous components. This analysis showed that a large portion of the variance in SO_2 oxidation rate was explained by the variance in ozone concentration. This photochemical component was generally much larger than the heterogeneous component. The following gas phase SO_2 oxidation rate expressions (in % per hour) represent the average for all the stations examined:

$$k_1 = 34\ [O_3] \text{ for St. Louis} \quad (2\text{-}53)$$

$$k_1 = 85\ [O_3] \text{ for Los Angeles} \quad (2\text{-}54)$$

where $[O_3]$ is the average hourly ozone concentration in ppm. These expressions generally predict SO_2 oxidation rates greater than predicted by ERT expression.

---

*NOTE: $k_1 = k_{1G} + k_{1A}$.

Gillani et al. (1981) derived a SO_2 oxidation rate expression which is applicable when relative humidity is less than 75% based on plume chemistry studies. This expression is

$$k_1 = 0.03\ R\ h\ [O_3] \qquad (2\text{-}55)$$

where

k_1 is SO_2 oxidation rate in % per hour,
R is total solar radiaton (kw/m^2),
h is plume depth (m) (minimum of z_i or $3\sigma_z$), and
$[O_3]$ is background ozone concentration (ppm).

It is important to note that this expression identifies essentially the same variables controlling SO_2 oxidation rate as the ERT expression. Figure 10 shows a comparison between SO_2 oxidation rates predicted with the Gillani et al. and ERT expressions for a range of conditions. These conditions include 8, 10, and 12 A.M. clear sky radiation in summer, fall, and winter; ozone concentration of 0.02 to 0.12 ppm; and a range of stability/mixing heights. The results show the two expressions predict comparable (within $\pm$30%) SO_2 oxidation rates. This result is quite significant since each equation was derived in an entirely different manner: Gillani et al. from observations, and ERT's from the kinetic model. The good agreement between the results provides additional confidence in both equations. However, since the ERT expression was generated from a wider range of conditions than the Gillani et al. expression, it is the preferred mechanism in MESOPUFF II.

The parameterized rate constant expressions discussed above apply only to daylight conditions. The gas phase free radical chemistry turns off at night. The expressions which employ ozone concentration and radiation levels as surrogate for OH concentration are inappropriate at night (Zak 1981). Nighttime oxidation of SO_2 and NO_2 to sulfates and nitrates, respectively, is believed to be slow due to the absence of OH. Observations of plume chemistry confirm this expectation. Figure 11 shows observed hourly conversion rates of SO_2 to $SO_4^=$ from eight plume studies as a

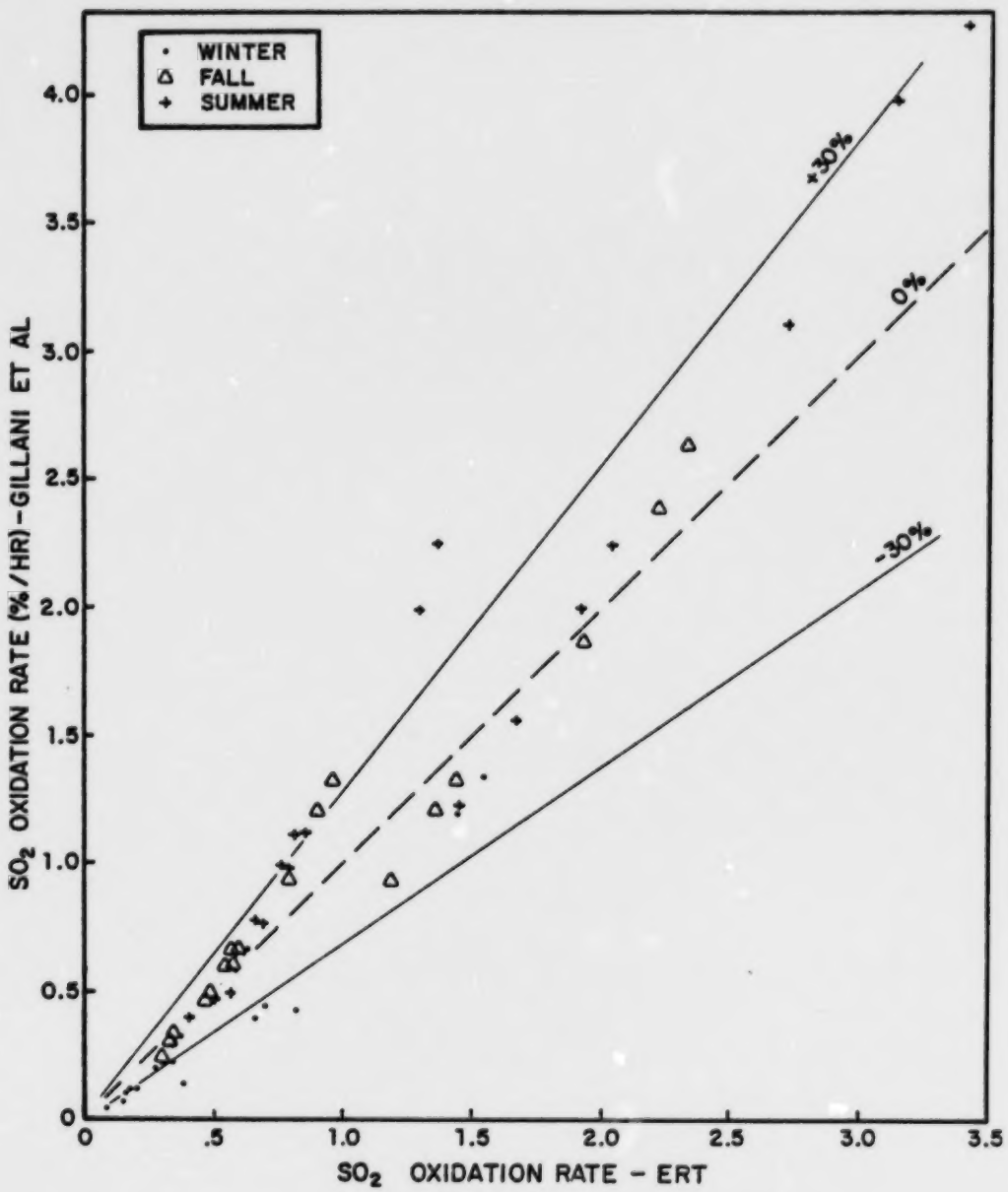

Figure 10 Comparison of SO_2 Oxidation Rates (% per Hour) Predicted by the ERT and Gillani et al. Expressions

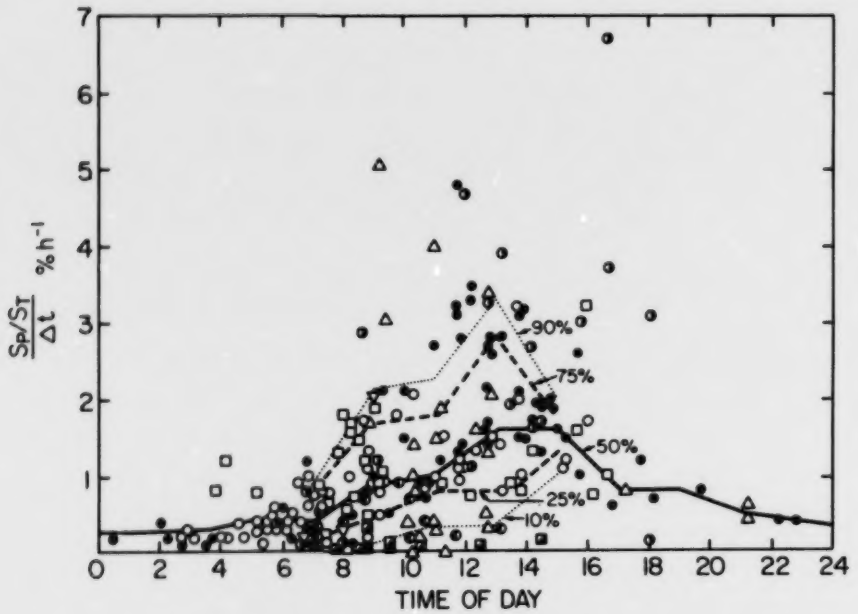

Figure 11 Average Plume Sulfur Conversion Rate as a Function of Mean Time of Day of Plume Transport. Only Data Corresponding to Plume Age Greater than 1.5 Hours are Plotted. Source: Wilson (1981)

function of time of day (Wilson 1981). These data show SO_2 oxidation rates are generally less than 0.5% per hour at night. Observed nighttime NO_x oxidation rates are also low. Forrest et al. (1981) found NO_x to total inorganic nitrate conversion rates in plumes of 0.1 to 3% per hour at night and during early morning hours. These low oxidation rates are presumably the result of heterogeneous reactions. Since these reactions are not well understood and, in general, are less important than daytime oxidation rates, constant oxidation rates are used in the model at night. Based on the results of plumes studies, oxidation rates of 0.2 and 2% per hour for SO_2 and NO_x, respectively, were selected for nighttime conditions in the MESOPUFF II chemical submodel.

2.4.3 Implementation of Chemistry

It is important to design air quality models with flexibilty and options to accommodate different applications and future improvements in scientific knowledge. Several options have been incorporated in the MESOPUFF II chemistry submodel to provide flexibility. First, in addition to the ERT expressions for SO_x and NO_x transformation rates, the submodel includes the Gillani et al. and Henry and Hidy expressions for SO_2 oxidation rates as options. Second, the model includes the option for external (user) specification of hourly transformation rates of reactions 1-3 (Equations 2-40 to 2-42). The user also has the options to specify hourly ozone data from a network of stations, a single ozone concentration for all hours, or use the default value of 80 ppb. Similarly, the user may use the default NH_3 concentration (10 ppb) and nighttime oxidation rates (see above) or specify values more appropriate for the application. Thus, the MESOPUFF II chemical submodel has ample flexibility to accommodate different applications and even different pollutants.

One of the problems in implementing chemistry in the puff modeling framework is that the model keeps track of puffs individually, yet atmospheric chemistry is a function of the concentrations from all puffs at a given location. This is particularly important for the NO_x chemistry, since the parameterized oxidation rate depends on NO_x concentration and

the NH_4NO_3 concentration depends on the total NH_3 and nitrate concentrations. Clearly, in a situation where puffs overlap, it would be incorrect to calculate the NO_x oxidation rate solely on the puff NO_x concentration and/or to calculate the particulate nitrate assuming all the ambient NH_3 would be available for one puff. Thus, the model has been designed to employ the local average NO_x concentration from all puffs in the NO_x oxidation rate expression for a single puff and apply the $HNO_3/NH_3/NH_4NO_3$ equilibrium relationship using the sum of total nitrate concentrations from all puffs and ammonia (total ammonia minus sulfate) at the location of interest.

2.5 Wet Removal

Numerous studies (e.g., Scott 1978, 1981; Garland 1978) have shown precipitation scavenging to be an efficient pollutant removal mechanism, especially for particulate pollutants such as $SO_4^=$ that serve as cloud condensation nuclei. Wet removal of soluble and reactive gaseous pollutants such as SO_2 and HNO_3 is also very important. Plumes can be nearly completely washed out by moderate rainfall within a few hours. During precipitation events, wet removal can easily dominate dry deposition in pollutant removal. On an annual basis, the average wet removal rates for SO_2 and HNO_3 in Eastern North America and Europe are comparable to those due to dry deposition (Scriven and Fisher 1975; Levine and Schwartz 1982); for $SO_4^=$ wet removal appears to be the more important removal mechanism (Scriven and Fisher 1975).

Wet removal includes both in-cloud scavenging (rainout) and below cloud scavenging (washout). The scavenging process is a complex one involving many factors. Scott (1978, 1981) has found precipitation scavenging of sulfate to be a strong function of the mechanism of precipitation formation and storm type (Figure 12). For example, the ratio of sulfate concentration in precipitation to that in air (i.e., the washout ratio, W) is 10-50 times larger for precipitation with growth due primarily to accretion than for precipitation growth due to vapor deposition. The scavenging efficiency of gases is a function of pollutant's solubility in water and reactivity.

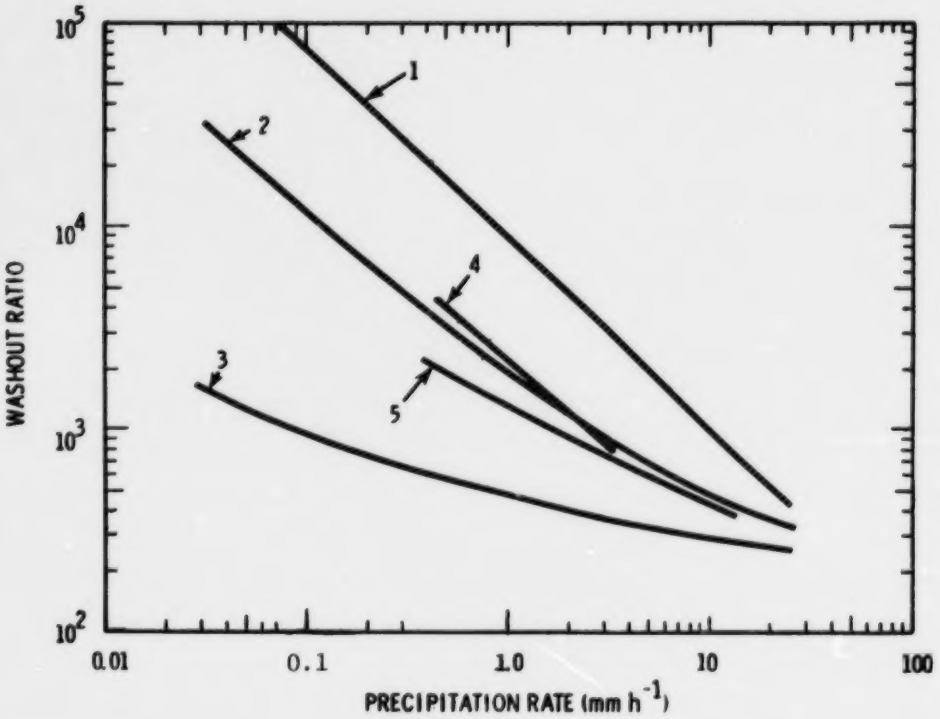

Figure 12 Washout Ratio as a Function of Precipitation Rate for Different Storm Types. Curve 1 Represents Predictions for Intense Convective Storms or from Clouds Whose Tops are Warmer than 0°C; Curve 2 Represents Predictions for Storms Where Rain Develops Without the Assistance of an Ice Growth Stage; Curve 3 is for Storms Where the Ice Growth Process is Necessary for Initiating Precipitation; Curve 4 is from Observed ^{24}Na Concentrations in Rainwater at Quillayute, Washington on 5, 6 April 1970; and Curve 5 is the Same as Curve 4 Except Curve for Data from 11 December 1969. Source: Scott (1978)

Barrie (1981) has shown SO_2 washout ratios to be strongly dependent on the pH of the rain and temperature (Figure 13).

However, a simple parameterization of wet removal suitable for order of magnitude wet removal estimates and using only routinely available meteorological variables is required in MESOPUFF II. A convenient approach compatible with the puff superposition principle is the scavenging coefficient formulation:

$$Q(t + 1) = Q(t) \exp [- \Lambda \Delta t] \quad (2\text{-}56)$$

where $Q(t)$, $Q(t + 1)$ is the mass (g) of pollutant in the puff at the beginning and end of the time step,

Λ is the scavenging ratio (s^{-1}), and

Δt is the time step (s).

Maul (1980) expresses Λ as:

$$\Lambda = \lambda \ (R/R_1) \quad (2\text{-}57)$$

where R is the rainfall rate (mm/hr),

R_1 is a reference rainfall rate of 1 mm/hr, and

λ is a scavenging coefficient (s^{-1}).

The rainfall rate used in Equation 2-57 is that observed at the closest surface station to the center of the puff. Table 7 contains the default values of the scavenging coefficient used in MESOPUFF II. Different values of λ are considered for liquid and frozen precipitation. Slinn et al. (1978) note that snow scavenging of gases is generally negligible. The scavenging coefficients for SO_2 and $SO_4^=$ removal by rain is based on Maul (1980) and Garland (1978). The scavenging coefficient for NO_3^- is believed to be roughly comparable to that for $SO_4^=$. Maul (1980) showed that values of $\lambda \sim 3\text{-}6 \times 10^{-5}\ s^{-1}$ can be derived for sulfate with the assumption of full removal from air entrained into the clouds. The high solubility and reactivity of HNO_3 suggests that a scavenging coefficient

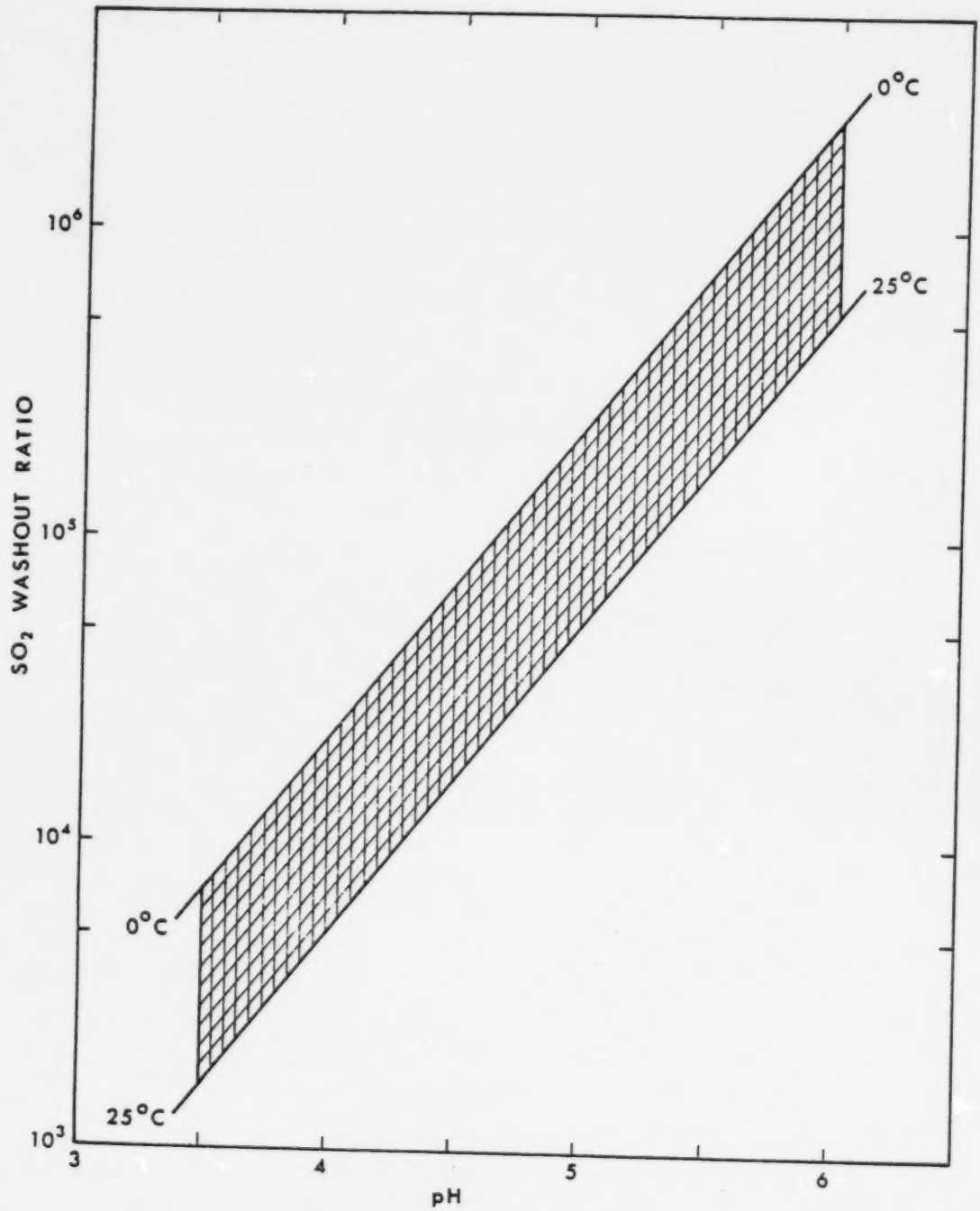

Figure 13 SO_2 Washout Ratio as a Function pH and Temperature for Equilibrium Scavenging Conditions
Source: Barrie (1981)

TABLE 7. DEFAULT VALUES OF THE SCAVENGING COEFFICIENT, λ (s^{-1})

Pollutant	Liquid Precipitation	Frozen Precipitation
SO_2	3×10^{-5}	0.0
$SO_4^=$	1×10^{-4}	3×10^{-5}
NO_x	0.0	0.0
HNO_3	6×10^{-5}	0.0
NO_3^-	1×10^{-4}	3×10^{-5}

similar to $SO_4^=$ is appropriate for HNO_3. Levine and Schwartz (1982) emphasize the sensitivity of HNO_3 removal to the raindrop size distribution, especially to the lower radii limit of the distribution because of the dominant contribution of the smaller drops to the removal rate. Their recommendations suggest a scavenging ratio of 6.5×10^{-5} s^{-1} for a rainfall rate of 1 mm/hr. Based on the low solubility of NO_x, a negligible scavenging coefficient is expected.

A precipitation code determined from the surface observations of precipitation type/intensity is used to determine if the value of λ for liquid or frozen precipitation is most appropriate. Precipitation observations are converted to precipitation codes as shown in Table 8. The liquid precipitation values of λ are used for precipitation codes 1-18; the frozen precipitation values are used for codes 19-45.

2.6 Puff Sampling Function

Puff superposition models such as MESOPUFF II represent a continuous plume with a number of discrete puffs. The concentration at a receptor is calculated by summing the contributions of each nearby puff, generally evaluated by taking a "snapshot" of each puff at particular time intervals (sampling steps) specified as a program input. The concentration at a receptor due to a horizontally symmetric with a Gaussian distribution is given by:

$$C(s) = \frac{Q(s)}{2\pi\sigma_y^2(s)} g(s) \exp\left[-\frac{r^2(s)}{2\sigma_y^2(s)}\right] \qquad (2\text{-}58)$$

$$g(s) = \frac{2}{\sqrt{2\pi}\sigma_z} \sum_{n=-\infty}^{\infty} \exp\left[-\frac{1}{2}\frac{(H_e + 2nz_i)^2}{\sigma_z^2(s)}\right] \qquad (2\text{-}59)$$

TABLE 8. CONVERSION OF REPORTED PRECIPITATION TYPE/INTENSITY TO PRECIPITATION CODES

Liquid Precipitation			Frozen Precipitation		
Precipitation Code	Type	Intensity	Precipitation Code	Type	Intensity
1	Rain	Light	19	Snow	Light
2	Rain	Moderate	20	Snow	Moderate
3	Rain	Heavy	21	Snow	Heavy
4	Rain Showers	Light	22	Snow Pellets	Light
5	Rain Showers	Moderate	23	Snow Pellets	Moderate
6	Rain Showers	Heavy	24	Snow Pellets	Heavy
7	Freezing Rain	Light	25	Not Used	-
8	Freezing Rain	Moderate	26	Ice Crystals	*
9	Freezing Rain	Heavy	27	Not Used	-
10	Not Used	-	28	Snow Showers	Light
11	Not Used	-	29	Snow Showers	Moderate
12	Not Used	-	30	Snow Showers	Heavy
13	Drizzle	Light	31	Not Used	-
14	Drizzle	Moderate	32	Not Used	-
15	Drizzle	Heavy	33	Not Used	-
16	Freezing Drizzle	Light	34	Snow Grains	Light
17	Freezing Drizzle	Moderate	35	Snow Grains	Moderate
18	Freezing Drizzle	Heavy	36	Snow Grains	Heavy
			37	Ice Pellets	Light
			38	Ice Pellets	Moderate
			39	Ice Pellets	Heavy
			40	Not Used	-
			41	Hail	*
			42	Not Used	-
			43	Not Used	-
			44	Small Hail	*
			45	Not Used	-

* Intensity not currently reported for ice crystals, hail and small hail.

where, $C(s)$ is the ground-level concentration,

s is the distance travelled by the puff,

$Q(s)$ is the mass of pollutant in the puff,

$\sigma_y(s)$ is the standard deviation of the Gaussian distribution in the horizontal,

$\sigma_z(s)$ is the standard deviation of the Gaussian distribution in the vertical,

$r(s)$ is the radial distance from the puff center,

z_i is the mixed-layer height, and

H_e is the effective height of the puff center.

The vertical term, $g(s)$ reduces to the uniformly mixed limit of $1/z_i$ for $\sigma_z/z_i \geq 1.6$. In general, puffs within the daytime mixed layer satisfy this criterion about an hour or two after release.

With Equation 2-58, an accurate representation of the continuous plume depends upon the puff release rate and sampling rate being sufficient to ensure that adjacent puffs overlap. Ludwig et al. (1977) have shown that if puff separation distances exceed $\sim 2\sigma_y$, inaccurate results may be obtained. The frequent sampling and/or puff release necessary to satisfy the $2\sigma_y$ criterion in the near-field of a source (where it is most restrictive) has a negative impact on model storage and computational requirements. Ludwig et al. (1977) recommend uniform space rather than uniform time release of puffs with a puff merging scheme to reduce the total number of puffs on the grid. However, frequent sampling or puff release is still necessary for near-field receptors. An alternate approach suggested by R. Yamartino (personal communication) and used in MESOPUFF II is to integrate Equation 2-58 over the distance of puff travel, Δs, during one sampling step.

$$\bar{C} = \frac{1}{\Delta s}\int_{s}^{s+\Delta s} \frac{Q(s)\, g(s)}{2\pi\, \sigma_y^{\,2}(s)} \exp\left[\frac{-r^2(s)}{2\sigma_y^{\,2}(s)}\right] ds \qquad (2\text{-}60)$$

If it is assumed that the most significant s dependence during the sampling step is in the r(s) and Q(s) terms, this integral can be evaluated. Assuming the trajectory segment is a straight line and transforming s to a dimensionless trajectory variable, p, results in:

$$r^2(p) = (X_t - X_r + p\Delta X)^2 + (Y_t - Y_r + p\Delta Y)^2 \qquad (2\text{-}61)$$

where p = 0,1 correspond to the beginning and end points of the trajectory (X_t, Y_t) and (X_{t+1}, Y_{t+1}), respectively, (X_r, Y_r) are the receptor coordinates, and ΔX, ΔY are the incremental X and Y distances travelled by the puff during the sampling step.

Equation 2-60 becomes:

$$\bar{C} = \frac{g}{2\pi\sigma_y^{\,2}} \int_0^1 Q(p) \exp\left[-\frac{r^2(p)}{2\sigma_y^{\,2}}\right] dp \qquad (2\text{-}62)$$

The exponential variation of Q due to removal and chemical transformation processes is expressed as a linear function over the sampling interval:

$$Q(p) = Q_t + p(Q_{t+1} - Q_t) \qquad (2\text{-}63)$$

Substituting Equation 2-63 into 2-62 results in:

$$\bar{C} = \frac{g}{2\pi\sigma_y^{\,2}} \quad Q_t \int_0^1 \exp\left[-\frac{r^2(p)}{2\sigma_y^{\,2}}\right] dp +$$

$$(Q_{t+1}-Q_t) \int_0^1 p \exp\left[-\frac{r^2(p)}{2\sigma_y^2}\right]dp \qquad (2\text{-}64)$$

The integrals in Equation 2-64 can be solved analytically and expressed in terms of error functions and exponentials.

$$\bar{C} = \frac{g}{2\pi\sigma_y^2}\left[Q_o I_1 + (Q_n - Q_o)\, I_2\right] \qquad (2\text{-}65)$$

$$I_1 = \sqrt{\frac{\pi}{2a}} \exp\left[1/2\,(b^2/a - c)\right] \left\{ \operatorname{erf}\left[\frac{a+b}{\sqrt{2a}}\right] - \operatorname{erf}\left[\frac{b}{\sqrt{2a}}\right] \right\} \qquad (2\text{-}66)$$

$$I_2 = -\frac{b}{a} I_1 + \frac{1}{a} \exp\left[1/2\,(b^2/a - c)\right] \left\{ \exp\left[-\tfrac{1}{2} b^2/a\right] - \exp\left[-\tfrac{1}{2}(a+2b+b^2/a)\right] \right\} \qquad (2\text{-}67)$$

$$a = (\Delta x^2 + \Delta y^2) / \sigma_y^2 \qquad (2\text{-}68)$$

$$b = [\Delta x(x_{t+1} - x_r) + \Delta y\,(y_{t+1} - y_r)]/\sigma_y^2 \qquad (2\text{-}69)$$

$$c = [(x_{t+1} - x_r)^2 + (y_{t+1} - y_r)^2]/\sigma_y^2 \qquad (2\text{-}70)$$

The vertical term, g, and σ_y are evaluated at the midpoint of the trajectory (p=0.5).

Because the integrated contribution of each puff over the sampling step is computed, this sampling function eliminates the problem of insufficient puff overlap. Table 9 contains the results of sampling tests performed with the conventional sampling algorithm (e.g., as in MESOPUFF) and the new sampling function used in MESOPUFF II. The analytic (straight-line) Gaussian solution is also shown. As expected, the conventional algorithm produces inaccurate results when the puff separation exceeds $2\sigma_y$. The puff separation is $u\delta t$, where u is the wind speed (5 m/s), δt is the

TABLE 9. EFFECT OF SAMPLING RATE, N, ON PREDICTED NEAR-FIELD (≤50 km) CONCENTRATIONS FOR TWO SAMPLING ALGORITHMS. PRESENTED ARE VALUES OF C/Q x10^7. N IS IN SAMPLES PER HOUR.

(Wind Speed - 5.0 m/s, PGT Stability D, Mixing Height = 1,000 m, Uniform Vertical Distribution)

Distance (km)	σ_y (m)	Straight Line Gaussian Eqn.	Conventional Sampling Algorithm					MESOPUFF II Sampling Algorithm				
			N=1	N=2	N=4	N=8	N=16	N=1	N=2	N=4	N=8	N=16
10	518	1.54	0.00	1.32	0.69	0.57	1.50	1.69	1.09	1.33	1.51	1.55
20	966	0.83	0.54	0.28	0.23	0.82	0.80	0.59	0.72	0.81	0.83	0.83
30	1,392	0.57	0.00	0.11	0.45	0.56	0.56	0.63	0.54	0.59	0.57	0.57
40	1,803	0.44	0.11	0.09	0.45	0.43	0.43	0.39	0.44	0.45	0.44	0.44
50	2,203	0.36	0.25	0.16	0.36	0.35	0.35	0.41	0.37	0.36	0.36	0.36

sampling interval (δt=3600s/N), and N is the sampling rate (samples per hour). The $2\sigma_y$ criterion is not satisfied for N=1 or 2 even at 50 km, resulting in 'gaps' in the concentration distribution. More accurate results are obtained with the MESOPUFF II algorithm. Acceptable results (i.e., within $\sim$ 5%) are obtained beyond 20 km with N=2 vs. N=8 for the conventional algorithm. The major source of error in the MESOPUFF II algorithm is due to the assumption of constant σ_y during the sampling interval. The value of σ_y is evaluated at the midpoint of the trajectory segment. Thus, during the first half of the trajectory σ_y is somewhat overestimated; during the second half, σ_y is underestimated. Because the length of each trajectory segment is proportional to the wind speed, this error may be minimized by increasing the sampling rate at higher wind speeds. MESOPUFF II offers the option to dynamically determine the sampling for each puff as follows:

$$N = 1 + \frac{u}{u_c} \qquad (2\text{-}71)$$

where u_c is a reference wind speed specified by the user. For example, for a u_c of 2 m/s, N will be assigned values of 1, 2, or 3 for values of u of 1.0, 2.0, and 4.0, respectively. The value of N given by Equation 2-71 is then compared to a user-specified minimum sampling rate; if lower, N is set equal to the minimum rate.

SECTION 3
DEMONSTRATION RUN

The MESOPUFF II model has been run for a two-day test period to allow a preliminary evaluation of the $SO_2 \rightarrow SO_4^=$ transformation mechanism and to qualitatively demonstrate the behavior of several other model algorithms. The modeled period was during the Tennessee Plume Study (TPS) which was conducted in August 1978 in the vicinity of the Cumberland Steam Plant in northwestern Tennessee (Schiermeier et al. 1979). The TPS is part of a larger EPA field program, called the Sulfur Transport and Transformation in the Environment (STATE) program, which was designed to examine the effects of SO_x emissions on regional scale sulfate concentrations.

Detailed measurements from aircraft traversing the Cumberland plume provided data on chemical processes and dispersion. Plumes from other TVA plants were also sampled when they were transported near the Cumberland plume. Plume trajectories were determined with aircraft and ground-level measurements of an injected tracer gas (SF_6), and by tracking tetroons and a manned LAMP balloon. Four specific scenarios were studied: (1) vertical mixing during highly convective conditions to downwind distances of 50 km; (2) horizontal plume spread during stable conditions with significant wind shear to downwind distances of 300-500 km; (3) dispersion during stable conditions to distances of 400 km; and (4) dispersion and chemical changes over a diurnal cycle, with fumigation in the morning and layering in the evening. The two-day study period (August 22-23) chosen for the test run falls under Scenario 4.

The model runs were made with a 24 x 30 grid covering the area encompassed by latitudes 35°-39° N and longitudes 86°-90° W (approximately from Memphis, Tennessee in the southwest corner of the grid to southern

Indiana in the northeast part of the grid). A grid spacing of 15 km was used. Only SO_x emissions from the Cumberland Steam Plant were modeled. Meteorological data from nine surface stations and three rawinsonde stations were processed (Figure 14). Special meteorological observations available during the TPS which would not be available for an operational application of the model (e.g., soundings made at 6-hour intervals) were not used. Mixed layer averaged winds were used to advect puffs within the mixed layer. Puffs above z_i were advected with vertically averaged winds through the layer from z_i to 700 mb. The surface depletion (3-layer) dry deposition model was used. Table 10 summarizes the model run parameters.

The time history of a particular puff through a diurnal cycle is presented in Table 11. The puff was released at 0100 CST on August 23 from the Cumberland stack. The puff quickly rose well above the shallow nocturnal boundary layer to a height of about 850 m. The rapid growth of the convective boundary layer and eventual fumigation of the puff is shown in Figure 15. Following the period of relatively slow puff growth, the puff quickly becomes uniformly mixed in the vertical after entrainment into the mixed layer. The puff growth rate while above the mixed layer is given by the E stability Turner dispersion curves.

Observed and predicted mixing heights in the vicinity of the Cumberland stack are presented in Figure 16. The model appears to correctly predict the growth of the morning convective mixed layer, although afternoon mixing heights are overpredicted. However, general conclusions regarding the quantitative performance of the mixing height algorithm should not be drawn from two case studies.

Modeling of dry deposition begins when the puff is fumigated into the mixed layer for the first time (1000-1100). Dry deposition and chemical transformation are of about equal importance as depletion mechanisms for SO_2 (loss rates of 1.5 - 2.5% per hour during daytime). The significance of boundary layer mixing as a limit to the deposition of pollutants is seen in the ratio v'_d/v_d. During the day when buoyancy-induced turbulence causes vigorous mixing, v'_d/v_d is nearly unity. However, during stable

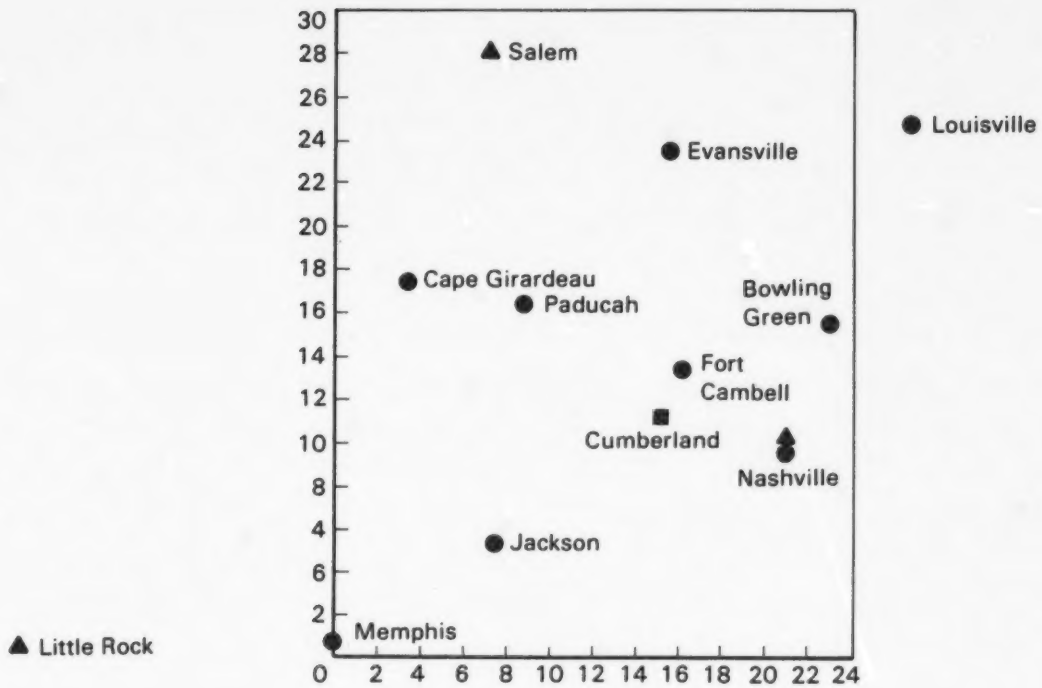

Figure 14 Location of Cumberland Steam Plant (■), Surface Meteorological Stations (●) and Upper Air Rawinsonde Stations (▲) on Meteorological Grid

8303066

TABLE 10. MODEL RUN PARAMETERS USED IN DEMONSTRATION RUN

Pollutants	SO_2, $SO_4^=$
Grid Size	24 x 30
Grid spacing	15 km
Time step	1 Hour
Sampling Rate	Variable - u_c = 2.0 m/s (see Equation 2-71) minimum rate = 4 (Aug. 22), 2 (Aug. 23)
Puff Release Rate	1 puff/hour
Background Ozone Concentration	80 ppb
Puff Growth Rate above Boundary Layer	E stability

TABLE 11. HISTORY OF PUFF RELEASED 8/23/78 HOUR 1

Hour (CST)	X_t (km)	σ_y (m)	σ_z (m)	z_i (m)	z_i(MAX) (m)	Puff Code [i]	K_1 [ii] (%/hr)	v_d (cm/s)	$\frac{v_d'}{v_d}$	K_d [iii] (%/hr)	$\frac{Q_m}{Q_t}$
1	0	1	1	-	-	3	-	-	-	-	0.
2	7	278	55	11	-	3	0.2	-	-	-	0.
3	17	603	82	29	-	3	0.2	-	-	-	0.
4	26	915	102	11	-	3	0.2	-	-	-	0.
5	37	1226	118	11	-	3	0.2	-	-	-	0.
6	47	1543	134	17	-	3	0.2	-	-	-	0.
7	58	1862	147	124	-	3	2.0	-	-	-	0.
8	69	2164	159	298	-	3	2.4	-	-	-	0.
9	79	2444	170	551	-	3	1.9	-	-	-	0.
10	88	2712	179	782	-	3	1.4	-	-	-	0.
11	99	3577	1703	955	955	1	2.4	0.82	1.00	2.9	1.0
12	117	5527	*	1120	1120	2	2.4	0.81	0.96	2.4	1.0
13	135	7326	*	1311	1311	2	2.2	0.83	0.96	2.3	1.0
14	155	9127	*	1417	1417	2	2.1	0.83	0.96	2.1	1.0
15	180	11002	*	1485	1485	2	2.0	0.85	0.96	2.0	1.0
16	201	12801	*	1510	1510	2	1.8	0.75	0.96	1.6	1.0
17	219	14527	*	1519	1519	2	1.0	0.83	0.95	1.8	1.0
18	235	16327	*	1497	1519	2	0.9	0.80	0.94	1.8	0.99
19	248	18127	*	1389	1519	2	0.6	0.28	0.47	0.3	0.91
20	259	19777	*	54	1519	6	0.2	0.28	0.26	0.1	0.03

*Puff Uniformly Mixed in Vertical - σ_z not calculated

[i] Puff codes: 1 = puff within mixed layer and Gaussian
2 = puff within mixed layer and uniform
3 = puff above mixed layer and Gaussian
6 = puff currently above (but previously below) mixed layer and uniform

[ii] K_1 = $SO_2 \rightarrow SO_4^=$ transformation rate

[iii] K_d = SO_2 dry deposition depletion rate

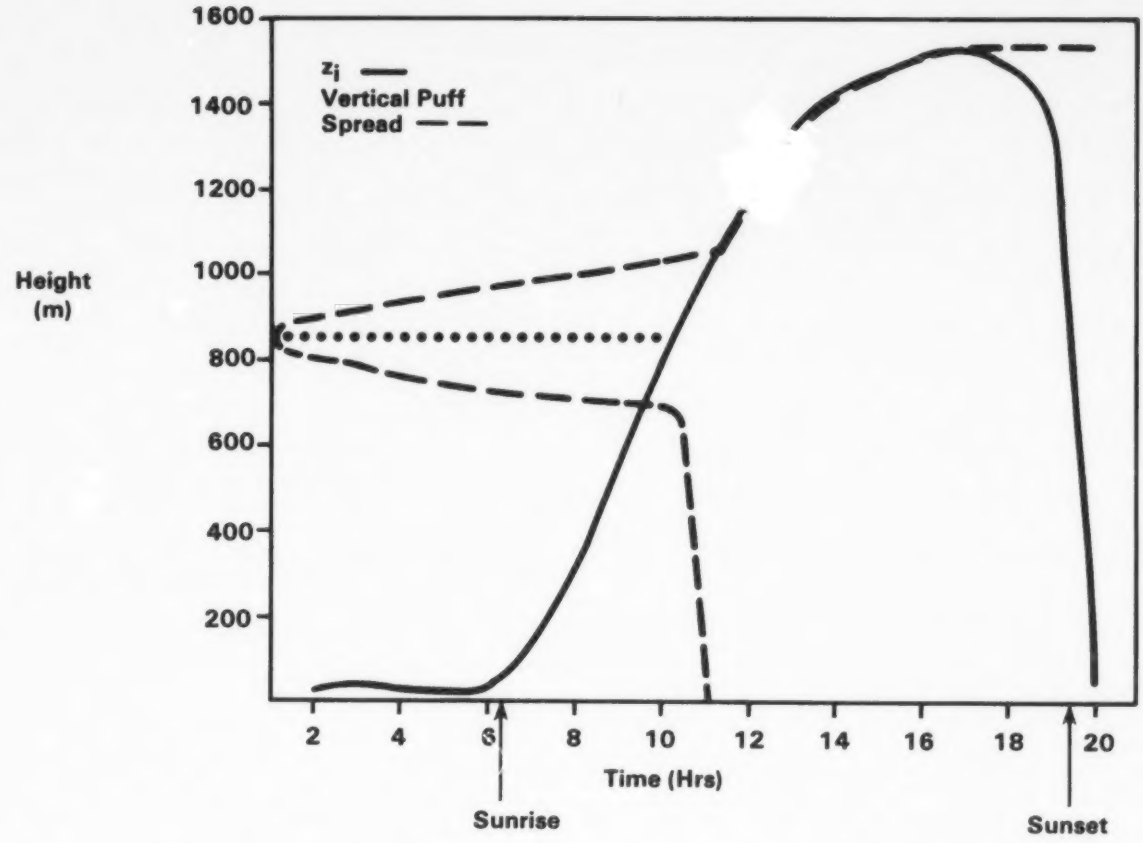

Figure 15 Boundary Layer Growth and Plume Fumigation

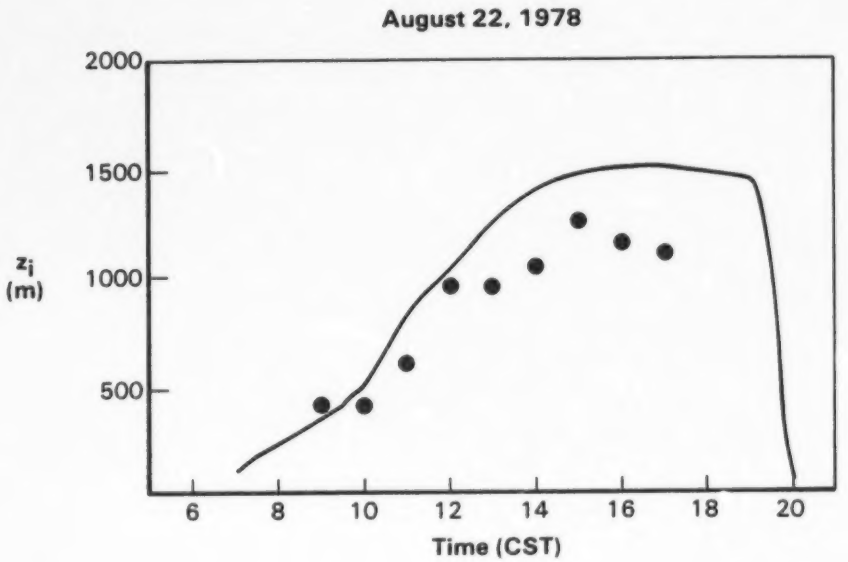

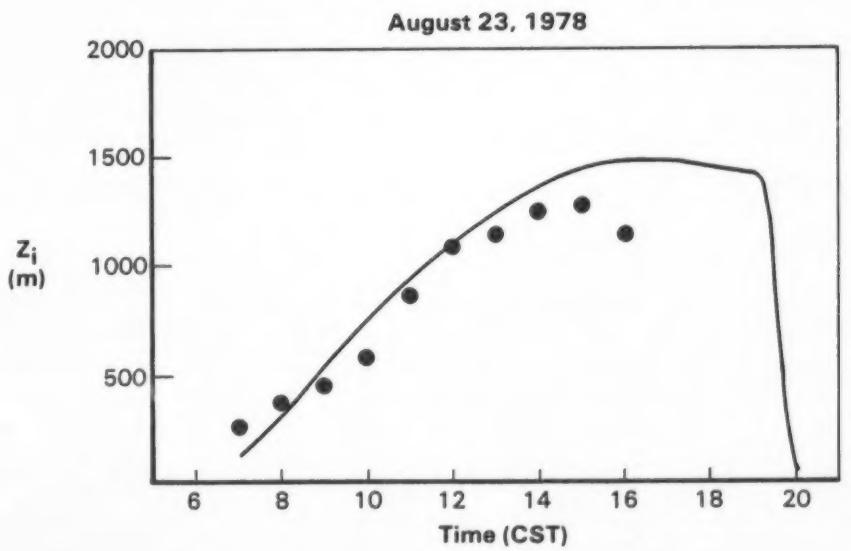

Figure 16 Observed (●) and Predicted (——) Mixing Heights in the Vicinity of the Cumberland Steam Plant

8304088

nighttime conditions, $v'_d/v_d << 1$, indicating the importance of the boundary layer mixing rate as an additional resistance to mass transfer. At 2000, the surface concentration (C_s) is only about 1/4 of the layer-averaged concentration (C_m). This lower near-surface concentration reduces dry deposition flux, thus increasing the lifetime of SO_2 in the atmosphere.

Predicted SO_2 to $SO_4^=$ conversion rates have been calculated and compared to observations reported by Gillani et al. (1981). The average conversion rate between the time of puff release and sampling is given by Gillani et al. (1981) as:

$$k_1 = \frac{C}{\Delta t} \frac{Q_{SO4}}{Q_t} \tag{3-1}$$

$$C_f = \frac{2}{1 + Q_{SO2}/Q_t} [1 - 0.5 \ln (Q_o/Q_t)] \tag{3-2}$$

where

k_1 is the average SO_2 to $SO_4^=$ conversion rate,

C_f is a correction factor accounting for changes in puff mass during the period of travel,

Q_o is the total initial sulfur mass in the puff (SO_2 + $SO_4^=$) weighted as SO_2,

Q_T is the total sulfur mass in the puff at the sampling time,

Q_{SO2} is the mass of SO_2 in the puff at the sampling time, and,

Q_{SO4} is the mass of SO_4 in the puff at the sampling time.

The MESOPUFF II conversion rates as well as those predicted by Gillani et al. (1981) are shown with observed rates in Table 12. Both schemes predict rates generally within the range of observed transformation rates during August 22. This day was generally sunny and relatively dry (low relative humidity). SO_2 oxidation was probably dominated by gas phase reactions. During August 23, however, a maritime tropical air mass characterized by high humidity and hazy conditions existed in the region.

TABLE 12. OBSERVED AND PREDICTED SO_2 CONVERSION RATES

DATE	Transport Time Obs. Plume (CST)	Plume Age (Hours)	Observed Rate (%/hour)	Predicted Rate (Gillani et al. 1981) (%/hour)	Transport Time Pred. Plume* (CST)	Plume Age (Hours)	Predicted Rate Eq. 2-49 and Eq. 2-52
8/22	2:55 - 6:25 2:50 - 6:50	3.5-4.0	0.1 - 0.45	0.05	3:00 - 6:45	3.75	0.59
	11:30 - 13:30	2.0	1.2 - 1.7	1.4 - 1.7	11:00 - 13:00	2.0	1.5
	11:00 - 14:30	3.5	1.5 - 1.8	1.9 - 2.0	11:00 - 14:30	3.5	1.7
8/23	6:30 - 10:30	4.0	1.7 - 2.8	0.3	6:00 - 10:00	4.0	2.0
	6:00 - 11:25	5.4	2.1 - 2.5	0.4	6:00 - 11:30	5.5	2.1
	5:15 - 15:15	10.0	2.7 - 2.9	0.9 - 1.0	5:00 - 15:00	10.0	1.9
	6:15 - 16:15	10.0	2.4 - 3.3	1.0 - 1.1	6:00 - 16:00	10.0	2.0

*Puffs released at hourly intervals

Low clouds increased during the day and dissipated after sunset. Significant plume-cloud interactions were reported by Gillani et al. (1981) during the late morning and early afternoon hours. The conversion rates predicted by MESOPUFF II are within the observed range during the morning transition period. However, the conversion rates averaged through the day are underpredicted, probably due to enhanced aqueous phase reactions associated with plume-cloud interactions. The empirical aqueous phase term of the rate equations is based on surface relative humidity measurements and is not able to account for these interactions. The Gillani et al. (1981) relationship is intended for conditions when gas phase reactions dominate (i.e., relative humidity < 75%). Therefore, it cannot account for the high observed rates during August 23 when liquid phase reactions contribute significantly.

In summary, MESOPUFF II modeling results for a limited two-day period during the TPS have been presented. The qualitative behavior of several model algorithms, including plume growth, development of the convective boundary layer, plume fumigation, and deposition processes have been presented. In particular, an encouraging preliminary evaluation of the SO_2 to $SO_4^=$ chemical transformation algorithm has been presented. These results represent only a brief and limited evaluation. Further evaluation with TPS data and additional regional-scale monitoring/ experimental measurement studies are recommended.

REFERENCES

Atkinson, R. and A.C. Lloyd 1980. "Evaluation of Kinetic and Mechanistic Data for Photochemical Smog Chamber Modeling", EPA Contract No. 68-02-3280, ERT Document No. P-A040.

Atkinson, R., A.C. Lloyd, L. Winges 1982. An Updated Chemical Mechanism for Hydrocarbon/NO_x/SO_x Photooxidations Suitable for Inclusion in Atmospheric Simulation Models, Atmos. Environ., 16, 1341.

Barrie, L.A. 1981. The Prediction of Rain Acidity and SO_2 Scavenging in Eastern North America. Atmos. Environ., 15, 31-41.

Benkley, C.W. and A. Bass 1979a. User's Guide to MESOPLUME Mesoscale Plume Segment Model. EPA 600/7-79-xxx, U.S. Environmental Protection Agency, Research Triangle Park, NC. 141 pp.

Benkley, C.W. and A. Bass 1979b. User's Guide to MESOPUFF (Mesoscale Puff Model. EPA 600/7-79-xxx, U.S. Environmental Protection Agency, Research Triangle Park, NC. 124 pp.

Benkley, C.W. and A. Bass 1979c. User's Guide to MESOPAC Mesoscale Meteorology Package). EPA 600/7-79-xxx. U.S. Environmental Protection Agency, Research Triangle Park, NC. 76 pp.

Briggs, G.A. 1975. Plume Rise Predictions. Lectures on Air Pollution and Environmental Impact Analyses. American Meteorological Society, Boston, MA, pp 59-111.

Brost, R.A. and J.C. Wyngaard 1978. A Model Study of the Stably Stratified Planetary Boundary Layer. J. Atmos. Sci. 35, 1427-1400.

Calvert, J.G., F. Su, J.W. Bottenheim and O.P. Strausz 1978. Mechanism of the Homogeneous Oxidation of Sulfur Dioxide in the Troposphere. Atmos. Environ., 12, 197.

Chamberlain, A.C. and R.C. Chadwick 1953. Deposition of Airborne Radio-Iodine Vapor. Nucleonics, 8, 22-25.

Deardorff, J.W. and Willis, G.E. 1975. A parameterization of diffusion into the mixed layer. J. Appl. Meteor., 14:1451-1458.

Draxler, R.R. 1977. A Mesoscale Transport and Diffusion Model. National Oceanic and Atmospheric Administration Tech. Memo. ERL-ARL-64, Air Resources Laboratories, Silver Springs, MD.

Draxler, R.R. 1979. Modeling the Results of Two Recent Mesoscale Dispersion Experiments. Atmos. Environ. 13, 1523-1533.

Fisher, B.E.A. 1980. Long-range Transport and Deposition of Sulfur Oxides. CERL internal report, Central Electricity Research Laboratories, Leatherhead, Surrey, United Kingdom.

Forrest, J., R.W. Garber and L. Newman 1981. Conversion Rates in Power Plant Plumes Based on Filter Pack Data: The Coal-fired Cumberland Plume. Atmos. Environ., 15, 2273.

Garland, J.A. 1978. Dry and wet removal of sulfur from the atmoshpere. Atmos. Environ., 12, 349-362.

Gifford, F.A. 1981. Horizontal Diffusion in the Atmosphere: A Lagrangian-Dynamical Theory. LA-8667-MS, Los Alamos Scient. Lab., P.O. Box 1663, Los Alamos, NM, 87545, 19 pp.

Gillani, N.V., S. Kohli and W.E. Wilson 1981. Gas-to-Particle Conversion of Sulfur in Power Plant Plumes: I. Parameterization of the Gas Phase Conversion Rates for Dry, Moderately Polluted Ambient Conditions. Atmos. Environ., 15, 2293-2313.

Hefter, J.L. 1965. The Variations of Horizontal Diffusion Parameters with Time for Travel Periods of One Hour or Longer. J. Appl. Meteor., 4, 153-156.

Hegg, D.A. and P.V. Hobbs 1981. Cloud Water Chemistry and the Production of Sulfate in Clouds. Atmos. Environ., 15, 1597-1604.

Henry, R.C., D.A. Godden, G.M. Hidy, and N.J. Lordi 1980. Simulation of Sulfur Oxide Behavior in Urban Areas. ERT Document P-A070-200. Prepared for the American Petroleum Institute.

Henry, R.C. and G.M. Hidy 1981. Discussion of Multivariate Analysis of Particulate Sulfate and Other Air Quality Variables, Part I. Annual data from Los Angeles and New York. Atmos. Environ., 15, 424.

Henry, R.C. and G.M. Hidy 1982. Multivariate Analysis of Particulate Sulfate and Other Air Quality Variables by Principle Components - II. Salt Lake City, Utah and St. Louis, Missouri. Atmos. Environ., 16, 929-943.

Hicks, B.B. and J.D. Shannon 1979. A method for modeling the deposition of sulfur by precipitation over regional scales. J. Appl. Meteor., 18, 1415-1420.

Hicks, B.B. 1982. Critical Assessment Document on Acid Deposition, Chapter VII - Dry Deposition. ATDL contribution file no. 81/24.

Horst, T.W. 1977. A Surface Depletion Model for Deposition from a Gaussian Plume. Atmos. Environ., 11, 41-46.

Levine, S.Z. and S.E. Schwartz 1982. In-Cloud and Below-Cloud of Scavenging of Nitric Acid Vapor. Atmos. Environ., 16, 1725-1734.

Ludwig, F.L., L.S. Gasidrek, and R.E. Ruff 1977. Simplification of a Gaussian Puff Model for Real-Time Minicomputer Use. Atmos. Environ., 11, 431-436.

Maahs, H.G. 1982. The Importance of Ozone in the Oxidation of Sulfur Dioxide in Nonurban Tropospheric Clouds. 2nd Symposium on the Composition of the Nonurban Troposphere, Amer. Meteorological Society, Williamsburg, VA, May 1982.

Martin, L.R., D.E. Damschen and H.S. Judeikis 1981. The Reactions of Nitrogen Oxides with SO_2 in Aqueous Aerosols. Atmos. Environ. 15:191-195.

Martin, L.R. 1982. Kinetic Studies of Sulfite Oxidation in Aqueous Solution, to be published in "SO_2, NO and NO_2 Oxidation Mechanisms: Atmospheric Considerations, ed. J.G. Calvert, Ann Arbor Science, Woburn, MA.

Maul, P.R. 1980. Atmospheric Transport of Sulfur Compound Pollutants. Central Electricity Generating Bureau MID/SSD/80/0026/R. Nottingham, England.

Morris, C.S., C.W. Benkley, and A. Bass 1979. User's Guide to MESOGRID (Mesoscale Grid) Model. EPA-600/7-79-xxx. U.S. Environmental Protection Agency, Research Triangle Park, NC. 118 pp.

Newman, L. 1981. Atmospheric Oxidation of Sulfur Dioxide: A Review as Viewed from Power Plant and Smelter Plume Studies. Atmos. Environ., 15, 2231.

Penkett, S.A., B.M.R. Jones, K.A. Brice and A.E.J. Eggleton 1979. The Importance of Atmospheric Ozone and Hydrogen Peroxide in Oxidizing Sulfur Dioxide in Cloud and Rainwater. Atmos. Environ., 13, 123-137.

Richards, L.W. et al., 1981. The Chemistry, Aerosol Physics, and Optical Properties of a Western Coal-Fired Power Plant Plume. Atmos. Environ., 15, 2111.

Schwartz, S.E., 1982. Gas-Aqueous Reactions of Sufur and Nitrogen Oxides in Liquid-Water Clouds; to be published in SO_2, NO and NO_2 Oxidation Mechanisms: Atmospheric Conditions, ed. J.G. Calvert. Ann Arbor Science, Woburn, MA.

Schwartz, S.E. and W.H. White 1982. Kinetics of Reactive Dosclution of Nitrogen Oxides into Aqueous Solution, in Advan. Environ. Sci. Technol., Vol. 12, S.E. Schwartz, Ed. (New York: Wiley and Sons, Inc., 1982).

Scire, J.S., J. Beebe, C. Benkley, and A. Bass 1979. User's Guide to the MESOFILE Postprocessing Package. EPA-600/7-79-xxx, U.S. Environmental Protection Agency, Research Triangle Park, N.C. 72 pp.

Scire J.S., F. Lurmann, A. Bass, and S. Hanna 1983. User's Guide to the MESCPUFF II Model and Related Processor Programs. U.S. Environmental Protection Agency, Research Triangle Park, NC.

Scott, B.C. 1978. Parameterization of sulfate removal by precipitation. J. Appl. Meteorol., 17, 1375-1389.

Scott, B.C. 1981. Sulfate Washout Ratios in Winter Storms. J. Appl. Meteor., 20, 619-625.

Scriven, R.A. and B.E.A. Fisher 1975. The long-range transport of airborne material and its removal by deposition and washout. Atmos. Environ., 9, 49-58.

Sehmel, G.A. 1980. Particle and Gas Dry Deposition - A review. Atmos. Environ. 14, 983-1011.

Sheih, C.M., M.L. Wesely, and B.B. Hicks 1979. Estimated Dry Deposition Velocities of Sulfur over the Eastern United States and Surrounding Regions. Atmos. Environ. 13 (10), 1361-1368.

Slinn, W.G., L. Hasse, B. Hicks, A Hogan, D. Lal, P. Liss, K. Munnich, G. Sehmel, and O. Vittori 1978. Some Aspects of the Transfer of Atmospheric Trace Constituents Past the Air-Sea Interface. Atmos. Environ., 12: 2055-2087.

Smith, F.B. 1981. The significance of wet and dry synoptic regions on long-range transport of pollution and its deposition. Atmos. Environ., 15, 863-873.

Stelson, A.W. and J.H. Seinfeld 1982. Relative Humidity and Temperature Dependence of the Ammonium Nitrate Dissociation Constant. Atmos. Environ., 16, 983-992.

Stelson, A.W., M.E. Bassett and J.H. Seinfeld 1983. Thermodynamic Equilibrium Properties of Aqueous Solutions of Nitrate, Sulfate and Ammonium. Acid Precipitation, Chemistry of Particles, Fog and Rain Volume. J. Teasley ed., Ann Arbor Science, Woburn, MA (in press).

Turner, D.B. 1964. A Diffusion Model for an Urban Area. J. Applied Meteorol., 3, 83-91.

Turner, D.B. 1970. Workbook of Atmospheric Dispersion Estimates. U.S. Dept. of H.E.W., Public Health Service, Pub. 999-AP-26, 88 pp.

U.S. EPA 1978. Guideline on Air Quality Models, OAQPS Guideline Series No. 1.2-080, EPA report No. EPA-450/2-78-027 (NTIS No. PB288783), 84 pp.

Van Ulden, A.P. 1978. Simple estimates for vertical diffusion from sources near the ground. Atmos. Environ., 12, 2152-2129.

Venkatram, A. 1980a. Estimating the Monin-Obukhov Length in the Stable Boundary Layer for Dispersion Calculations. Boundary-Layer Meteorology 19, 481-485.

Venkatram, A. 1980b. Estimation of turbulence velocity scales in the stable and the unstable boundary layer for dispersion applications. In: Eleventh NATO-CCSM International Technical Meeting on Air Pollution Modeling and its Application 54-56.

Venkatram, A., B.E. Ley and S.Y. Wong 1982. A statistical model to estimate long-term concentrations of pollutants associated with long-term transport. Atmos. Environ., 16, 249-257.

Wang, I.T. and P.C. Chen 1980. Estimations of Heat and Momentum Fluxes Near the Ground. Proc. 2nd Joint Conf. on Applications of Air Poll. Meteorology, New Orleans. LA, March 24-27. pp 764-769.

Wesely, M.L., and B.B. Hicks 1977. Some factors that Affect the Deposition Rates of Sulfur Dioxide and Similar gases on Vegetation. J. Air Poll. Control Assoc. 27, pp 1110-1116.

Wilson, W.E. 1981. Sulfate Formation in Point Source Plumes: A Review of Recent Field Studies. Atmos. Environ., 15, 2573.

Zak, B.D. 1981. Lagrangian Measurements of Sulfur Dioxide to Sulfate Conversion Rates. Atmos. Environ., 15, 2583.

APPENDIX A

REACTIONS AND RATE CONSTANTS OF THE ATKINSON et al. (1982) CHEMICAL MECHANISM

Reaction	Rate Constant (ppm min units)
Inorganics	
1. $NO_2 \rightarrow h\nu \xrightarrow{O_2} NO + O_3$	k_1 variable
2. $NO + O_3 \rightarrow NO_2 + O_2$	$k_2 = 1.0 \times 10^6\ T^{-1}\ e^{-1450/T}$
3. $O_3 + h\nu \rightarrow 2\ OH$	$k_3 = \beta_1 k_1 \times 7.6 \times 10^{-6}\ [H_2O]$
4. $OH + NO \overset{M}{\rightarrow} HONO$	$k_4 = 8.7 \times 10^8\ T^{-2}$
5. $OH + NO_2 \overset{M}{\rightarrow} HNO_3$	$k_5 = 1.5 \times 10^9\ T^{-2}$
6. $HONO + h\nu \rightarrow OH + NO$	$k_6 = \beta_2 k_1$
7. $HO_2 + NO \rightarrow OH + NO_2$	$k_7 = 3.7 \times 10^6\ T^{-1}$
8. $HO_2 + NO_2 \overset{M}{\rightarrow} HO_2NO_2$	$k_8 = 1.5 \times 10^8\ T^{-2}$
9. $HO_2NO_2 \overset{M}{\rightarrow} HO_2 + NO_2$	$k_9 = 7.8 \times 10^{15}\ e^{-10420/T}$
10. $HO_2 + HO_2 \rightarrow H_2O_2 + O_2$	$k_{10} = 3.4 \times 10^4\ T^{-1}\ e^{1100/T}$ + $[H_2O]\ 5.8 \times 10^{-5}\ T^{-2}\ e^{5800/T}$
11. $H_2O_2 + h\nu \rightarrow 2OH$	$k_{11} = \beta_3 k_1$
12. $OH + CO \xrightarrow{O_2} HO_2$	$k_{12} = 1.3 \times 10^5\ T^{-1}$
13. $NO_2 + O_3 \rightarrow NO_3$	$k_{13} = 5.3 \times 10^4\ T^{-1}\ e^{-2450/T}$
14. $NO + NO_3 \rightarrow 2NO_2$	$k_{14} = 8.4 \times 10^6\ T^{-1}$
15. $NO_2 + NO_3 \overset{M}{\rightarrow} N_2O_5$	$k_{15} = 3.1 \times 10^7\ T^{-1}\ e^{-1100/T}$
16. $N_2O_5 \overset{M}{\rightarrow} NO_2 + NO_3$	$k_{16} = 3.5 \times 10^{18}\ e^{-12280/T}$
17. $N_2O_5 + H_2O \rightarrow 2HNO_3$	$k_{17} = 6.7 \times 10^{-4}\ T^{-1}$
18. $NO_3 + h\nu \rightarrow 0.3\ NO + 0.7\ NO_2 + 0.7\ O_3$	$k_{18} = \beta_4 k_1$

Reaction	Rate Constant (ppm min units)
19. $OH + O_3 \rightarrow HO_2$	$k_{19} = 7.0 \times 10^5\ T^{-1}\ e^{-940/T}$
20. $HO_2 + O_3 \rightarrow OH$	$k_{20} = 4.8 \times 10^3\ T^{-1}\ e^{-680/T}$
Formaldehyde	
21. $HCHO + h\nu \xrightarrow{O_2} HO_2 + HO_2 + CO$	$k_{21} = \beta_5 k_1$
22. $HCHO + h\nu \rightarrow CO + H_2$	$k_{22} = \beta_6 k_1$
23. $OH + HCHO \xrightarrow{O_2} HO_2 + CO$	$k_{23} = 4.4 \times 10^6\ T^{-1}$
Acetaldehyde	
24. $CH_3CHO + h\nu \xrightarrow{O_2} CH_3O_2 + HO_2 + CO$	$k_{24} = \beta_7 k_1$
25. $OH + CH_3CHO \xrightarrow{O_2} CH_3CO_3$	$k_{25} = 3.0 \times 10^6\ T^{-1}\ e^{250/T}$
26. $CH_3CO_3 + NO_2 \rightarrow PAN$	$k_{26} = 2.1 \times 10^6\ T^{-1}$
27. $PAN \rightarrow CH_3CO_3 + NO_2$	$k_{27} = 1.2 \times 10^{18}\ e^{-13543/T}$
28. $CH_3CO_3 + NO \xrightarrow{O_2} NO_2 + CH_3O_2$	$k_{28} = 3.1 \times 10^6\ T^{-1}$
29. $CH_3O_2 + NO \rightarrow HCHO + HO_2 + NO_2$	$k_{29} = 3.1 \times 10^6\ T^{-1}$
Propane	
30. $OH + PROPANE \rightarrow PO_2$	$k_{30} = 6.6 \times 10^6\ T^{-1}\ e^{-680/T}$
31. $PO_2 + NO \rightarrow HO_2 + NO_2 + CH_3COCH_3$	$k_{31} = 3.1 \times 10^6\ T^{-1}$
Alkanes	
32. $OH + ALKANE \rightarrow AO_2$	$k_{32} = 8.0 \times 10^6\ T^{-1}\ e^{-560/T}$ for explicit n-butane $k_{32} = 6.6 \times 10^6\ T^{-1}\ e^{-400/T}$ for lumped $\geq C_4$ alkane

Reaction	Rate Constant (ppm min units)
33. $AO_2 + NO \rightarrow 1.3\ NO_2 - + -0.4\ NO + 0.9\ HO_2 + 0.6\ CH_3CHO + 0.1\ RCHO + 0.5\ MEK$	Explicit n-butane $\rightarrow 1.7\ NO_2 + -0.8\ NO + 0.9\ HO_2 + 0.15\ HCHO + 0.3\ CH_3CHO + 0.1\ RCHO + 0.3\ CH_3COCH_3 + 0.45\ MEK$ Lumped $\geq C_4$ alkane mechanism $k_{33} = 3.1 \times 10^6\ T^{-1}$ for both systems

Higher Aldehydes

34. $OH + RCHO \xrightarrow{O_2} RCO_3$	$k_{34} = 9.2 \times 10^6\ T^{-1}$
35. $RCO_3 + NO_2 \rightarrow PPN$	k_{35} $2.1 \times 10^6\ T^{-1}$
36. $PPN \rightarrow RCO_3 + NO_2$	$k_{36} = 1.2 \times 10^{18}\ e^{-13543/T}$
37. $RCO_3 + NO \rightarrow C_2H_5O_2 + NO_2$	$k_{37} = 3.1 \times 10^6\ T^{-1}$
38. $C_2H_5O_2 + NO \xrightarrow{O_2} CH_3CHO + HO_2 + NO_2$	$k_{38} = 3.1 \times 10^6\ T^{-1}$
39. $RCHO + h\nu \xrightarrow{O_2} C_2H_5O_2 + CO + HO_2$	$k_{39} = \beta_8 k_1$

Ketones

40. $OH + MEK \xrightarrow{O_2} XO_2$	$k_{40} = 4.4 \times 10^6\ T^{-1}\ e^{-330/T}$
41. $XO_2 + NO \rightarrow NO_2 + CH_3CHO + CH_3CO_3$	$k_{41} = 3.1 \times 10^6\ T^{-1}$
42. $MEK + h\nu \xrightarrow{O_2} CH_3CO_3 + C_2H_5O_2$	$k_{42} = \beta_9 k_1$
43. $CH_3COCH_3 + h\nu \xrightarrow{O_2} CH_3CO_3 + CH_3O_2$	$k_{43} = \beta_{10} k_1$

Reaction	Rate Constant (ppm min units)
Alkenes	
44. $OH + Ethene \xrightarrow{O_2} 2HCHO + HO_2$	$k_{44} = 9.7 \times 10^5\ T^{-1}\ e^{380/T}$
45. $OH + Propene \xrightarrow[NO_2 - NO]{O_2} HCHO + CH_3CHO + HO_2$	$k_{45} = 1.8 \times 10^6\ T^{-1}\ e^{540/T}$
46. $OH + Butene \xrightarrow[+ NO_2 - NO]{O_2} 1.8\ CH_3CHO + 0.9\ HO_2$	$k_{46} = 5.0 \times 10^6\ T^{-1}\ e^{540/T}$
47. $O_3 + Ethene \rightarrow HCHO + 0.4\ \dot{C}H_2\dot{O}_2 + 0.4\ CO + 0.12\ HO_2$	$k_{47} = 4.2 \times 10^3\ T^{-1}\ e^{-2560/T}$
48. $O_3 + Propene \rightarrow 0.5\ HCHO + 0.5\ CH_3CHO + 0.2\ \dot{C}H_2\dot{O}_2 + 0.2\ CH_3\dot{C}HO\dot{O} + 0.3\ CO + 0.2\ HO_2 + 0.1\ OH + 0.2\ CH_3O_2$	$k_{48} = 3.1 \times 10^3\ T^{-1}\ e^{-1900/T}$
49. $O_3 + Butenes \rightarrow CH_3CHO + 0.4\ CH_3\dot{C}HO\dot{O} + 0.3\ HO_2 + 0.2\ OH + 0.45\ CH_3O_2 + 0.2\ CO$	$k_{49} = 3.3 \times 10^3\ T^{-1}\ e^{-1050/T}$
50. $\dot{C}H_2\dot{O}_2 + NO \rightarrow HCHO + NO_2$	$k_{50} = 3.1 \times 10^6\ T^{-1}$
51. $\dot{C}H_2\dot{O}_2 + NO_2 \rightarrow HCHO + NO_2$	$k_{51} = 3.1 \times 10^5\ T^{-1}$
52. $\dot{C}H_2\dot{O}_2 + SO_2 \rightarrow HCHO + SO_4^{=}$	$k_{52} = 3.0 \times 10^4 T^{-1}\ T^{-1}$
53. $\dot{C}H_2\dot{O}_2 + H_2O \rightarrow Product$	$k_{53} = 1.5\ T^{-1}$
54. $CH_3\dot{C}HO\dot{O} + NO \rightarrow CH_3CHO + NO_2$	$k_{54} = 3.1 \times 10^6\ T^{-1}$
55. $CH_3\dot{C}HO\dot{O} + NO_2 \rightarrow CH_3CHO + NO_3$	$k_{55} = 3.1 \times 10^5\ T^{-1}$
56. $CH_3\dot{C}HO\dot{O} + SO_2 \rightarrow CH_3CHO + SO_4^{=}$	$k_{56} = 3.0 \times 10^4\ T^{-1}$
57. $CH_3\dot{C}HO\dot{O} + H_2O \rightarrow Product$	$k_{57} = 1.5\ T^{-1}$

Reaction	Rate Constant (ppm min units)
Aromatics	
58. OH + Benzene → 0.25 Cresol + 0.25 HO_2 + 0.75 ADD	$k_{58} = 5.3 \times 10^5\ T^{-1}$
59. OH + Toluene → 0.15 ARO_2 + 0.20 Cresol + 0.20 HO_2 + 0.65 ADD	$k_{59} = 2.7 \times 10^6\ T^{-1}$
60. OH + Xylene → 0.25 Cresol + 0.25 HO_2 + 0.75 ADD	$k_{60} = 7.9 \times 10^6\ T^{-1}$ for lumped xylene $= 1.05 \times 10^7\ T^{-1}$ for explicity m-xylene
61. ADD + NO → 0.75 NO_2 + 0.75 HO_2 + 0.75 DIAL + α_1 $(CHO)_2$ + α_2 CH_3COCHO	$k_{61} = 3.1 \times 10^6\ T^{-1}$
62. OH + DIAL → E1	$k_{62} = 1.3 \times 10^7\ T^{-1}$
63. E1 + NO_2 → E1 NO_2	$k_{63} = 2.1 \times 10^6\ T^{-1}$
64. E1 NO_2 → E1 + NO_2	$k_{64} = 1.2 \times 10^{18}\ e^{-13543/T}$
65. E1 + NO → 3 NO_2 -2 NO + $\alpha_3(CHO)_2$ + α_4 CH_3CO_3 + α_4 CH_3COCHO + α_3 CO + $\alpha_3 HO_2$	$k_{65} = 3.1 \times 10^6\ T^{-1}$
66. OH + $(CHO)_2$ $\xrightarrow{O_2}$ HO_2 + CO	$k_{66} = 8.8 \times 10^6\ T^{-1}$
67. $(CHO)_2$ + hν → HCHO + CO	$k_{67} = \beta_{11} k_1$
68. OH + CH_3COCHO $\xrightarrow{O_2}$ CH_3CO_3 + CO	$k_{68} = 6.6 \times 10^6\ T^{-1}$
69. CH_3COCHO + hν $\xrightarrow{O_2}$ CH_3CO + HO_2 + CO	$k_{69} = \beta_{12} k_1$

	Reaction	Rate Constant (ppm min units)
70.	$OH + Cresol \rightarrow ADD2$	$k_{70} = 1.9 \times 10^{7}\ T^{-1}$
71.	$ADD2 + NO \rightarrow 0.75\ NO_2 + 0.75\ HO_2 + 0.75\ DIAL$	$k_{71} = 3.1 \times 10^{6}\ T^{-1}$
72.	$NO_3 + Cresol \rightarrow HNO_3 + Phenoxy$	$k_{72} = 6.6 \times 10^{6}\ T^{-1}$
73.	$Phenoxy + NO_2 \rightarrow Products$ (o-, p-nitrophenols)	$k_{73} = 6.6 \times 10^{6}\ T^{-1}$
74.	$ARO_2 + NO \rightarrow 0.75\ NO_2 + 0.75\ HO_2 + 0.75\ ARCHO$	$k_{74} = 3.1 \times 10^{6}\ T^{-1}$
75.	$ARCHO + h\nu \rightarrow Products$	$k_{75} = \beta_{13} k_1$
76.	$OH + ARCHO \xrightarrow{O_2} ARCO_3$	$k_{76} = 5.7 \times 10^{6}\ T^{-1}$
77.	$ARCO_3 + NO_2 \rightarrow PBZN$	$k_{77}\ 2.1 \times 10^{6}\ T^{-1}$
78.	$PBZN \rightarrow ARCO_3 + NO_2$	$k_{78} = 1 \times 10^{17}\ e^{-13025/T}$
79.	$ARCO_3 + NO \rightarrow PhO_2 + NO_2$	$k_{79} = 3.1 \times 10^{6}\ T^{-1}$
80.	$PhO_2 + NO \rightarrow Phenoxy + NO_2$	$k80\ 3.1 \times 106\ T^{-1}$
	$\underline{SO_2}$	
81.	$OH + SO_2 \xrightarrow{M} SO_4^{=}$	$k_{81} = 1.5 \times 10^{13}\ T^{-4}$

NOTES

1) β_i = proportionality of photolytic rate for the ith photolytic reaction rate to k_1. β_i are a function of solar zenith angle.

2) α_i = variable stoichiometric coefficients which depend on the benzene, toluene, and xylene concentrations.